OPTICAL AND ELECTRICAL CHARACTERISATION OF P3HT:PCBM ORGANIC PHOTOVOLTAIC DEVICES

OKPOWE, OMENA

A PROJECT SUBMITTED IN PARTIAL FUFILLMENT OF THE REQUIREMENTS FOR THE AWARD OF A MASTER OF SCIENCE DEGREE IN MATERIALS SCIENCE

AFRICAN UNIVERSITY OF SCIENCE AND TECHNOLOGY

ABUJA

2010

DEDICATION

To my dear mum.

Her care and support have been my greatest sources of inspiration daily.

ACKNOWLEDGEMENTS

I would like to thank my supervisor, Professor Wole Soboyejo, for his time, help and advice during the duration of this study despite his very busy schedule. It has been a great experience working with him and a privilege having him as my supervisor.

I am also indebted to Dr Zebaze Kana who actually made this work become a reality. Discussions with him always brought up interesting ideas for new studies and possible interpretations of the observed data. His inspiration and 'never say die attitude' actually encouraged me to keep strong till the very end.

A special thank you go to Professors E.O.B. Ajayi(who is the reason for my undergoing a masters program at AUST), H.B. Olaniyi, (who has been a mentor and role model to me), Professor K. Osseo Asare, D. Buttery, T Debroy and D. Radev for their various contributions to my academic progress thus far. Their teachings and approach to science have continually motivated me to carry on.

I will also like to appreciate Tiffany Tong, Wali Akande, Olufemi Emmanuel, Zakari Abdullahi, Deborah Olalekan, Oyebimpe Yusuf, Adedoyin Adegoke, Joseph Asare, Botah Richard and my colleagues in materials science stream Damilola Momodu, Auphedeous Dang-I, Mustapha Kabir, Aymar Doumingou and Frank Nsaful for their various contributions in one way or the other to the successful completion of this project.

I would like to give special thanks to my mum, Mrs Ifenedo-Okpowe(for always sending the right words at the right times), my immediate family members- C. Okpowe, Efe, Ovie, Tarhe, Edirin, Runo, Asa, Ukpong and Vona for their prayers and immeasurable support all through my program.

Finally and above all, I will like to appreciate my God and Father for granting me the grace to see through to the very end of this project.

TABLE OF CONTENTS

LIST OF FIGURES

LIST OF TABLES

INTRODUCTION

1.1 BACKGROUND

The numerous limitations of inorganic solar cells has led to keen interest and exploitation of organic solar cells in recent times. They offer several advantages such as lightness, mechanical flexibility, low production cost, ease of processing and have a high potential for large area solar conversion[1].

The properties, performance and lifespan of these solar cells depend on the properties of the active layer and interface between the components[1]. Thus far research efforts have been focused on flexibility, colour for building integration, transparency and tackling some of the challenges limiting the industrial applications of organic solar cells[22] especially their low efficiencies.

The efficiency that can be reached with single junction cells is currently in the neighbourhood of 5% while the predictions of the theoretically and practically accessible power conversion efficiencies are predicted to be about twice the value or even higher. The best active layer materials thus far recorded are PCBM:P3HT which still have only about 6.5% efficiency[11]. Aside from the efficiency, there are at least two other factors critical to the success of polymer and organic solar cells, which summarized in Fig. 1.1 as the unification challenge. The important aspects other than the power conversion efficiency that have been identified are the stability and the processing .[44]

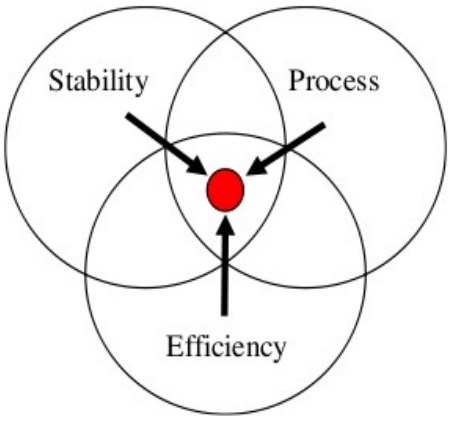

Fig1.1: Unifying efficiency, Stability and Fabrication process. A recipe for the success of polymer and organic solar cells[44]

These individual areas have been given relatively minimal consideration. Most especially the rather poor device stability of organic solar cells has been given little attention. Inorganic silicon-based solar cells may last on the order of 25 years; so in this respect, organic devices must be improved tremendously to become technologically interesting. Organic materials for instance are by nature

more susceptible to chemical degradation from oxygen and water than inorganic materials. A number of studies have been carried out and they show that the stability/degradation issue is rather complicated and certainly not yet fully understood though progress has been made. A particular property that affects the efficiency and degradation of these cells is the morphological features of the layers especially the active layer and the charge transport. These are also looked into in this work through relevant characterisation techniques.

1.2 STATEMENT OF PROBLEM

The recombination of carriers before they reach the anode and cathode has stimulated an interest in fast charge carriers that can reduce the amount of recombination. There is also a need to study the stability of the micro-structures under charge transport conditions. This is what this work is aimed at contributing to.

1.3 SCOPE OF THE STUDY

This project entails the fabrication and characterisation of some organic solar cell models which have the potential of improving the charge carrier characteristics of organic solar cells. The stability of the solar cell structures will also be studied based on their current voltage characteristics. Whereas this chapter gives an introduction to this work, previous works on organic and hybrid organic/inorganic solar cells are reviewed in chapter 2. Results from the current study are presented and discussed in chapter 3 while the final chapter entails some conclusions and suggestions for future work.

LITERATURE REVIEW

2.1 ORGANIC SOLAR CELLS

Organic photovoltaics are planar cells with an organic light absorbing layer sandwiched between two different electrodes. One of the electrodes is usually semi-transparent so as to allow light pass through. Indium tin oxide (ITO) is used as the anode while the cathode is usually a low work function metal such as aluminium although, Ca, Mg and Au are sometimes used.

The active layer is usually made up of large conjugated systems i.e. carbon atoms covalently bonded with alternating single and double bonds. The pz electronic orbitals de-localize, forming a π bonding and π* antibonding orbital. The collection of de-localized π orbitals make up the HOMO while that of the π* make up the LUMO. Between these two, lie a bandgap that is typically 1-4eV.

2.1.1 PHOTOEXCITATION IN ORGANIC SOLAR CELLS

The energy gap is typically within the range of visible photons i.e. 200 nm-1300 nm. Upon illumination, electrons are promoted to the LUMO leaving behind a hole in the HOMO level. After photon absorption, a singlet or a polaron may form.

A singlet exciton forms by an electron hole pair held by electrostatic attraction in the same polymer chain. Their energy levels are located within the bandgap and they have a very short lifetime after which they recombine. A polaron however is less predominant than a singlet. When a charge is added to a polymer chain, it deforms to lower the energy of the carrier. They both constitute a polaron P^+or P^- depending on the sign of the charge. These polarons then drift along the conjugated chain and on reaching an end, hop to another chain.

2.1.2 TYPES OF ORGANIC SOLAR CELLS

Single layer, bilayer and dispersed heterojunction cells (DHC) have been produced (Fig 1a, 1b &1c.). Single layers have just a single active layer where photo-excitation takes place while bilayer cells have two separate layers one serving as acceptor the other as a donor layer.

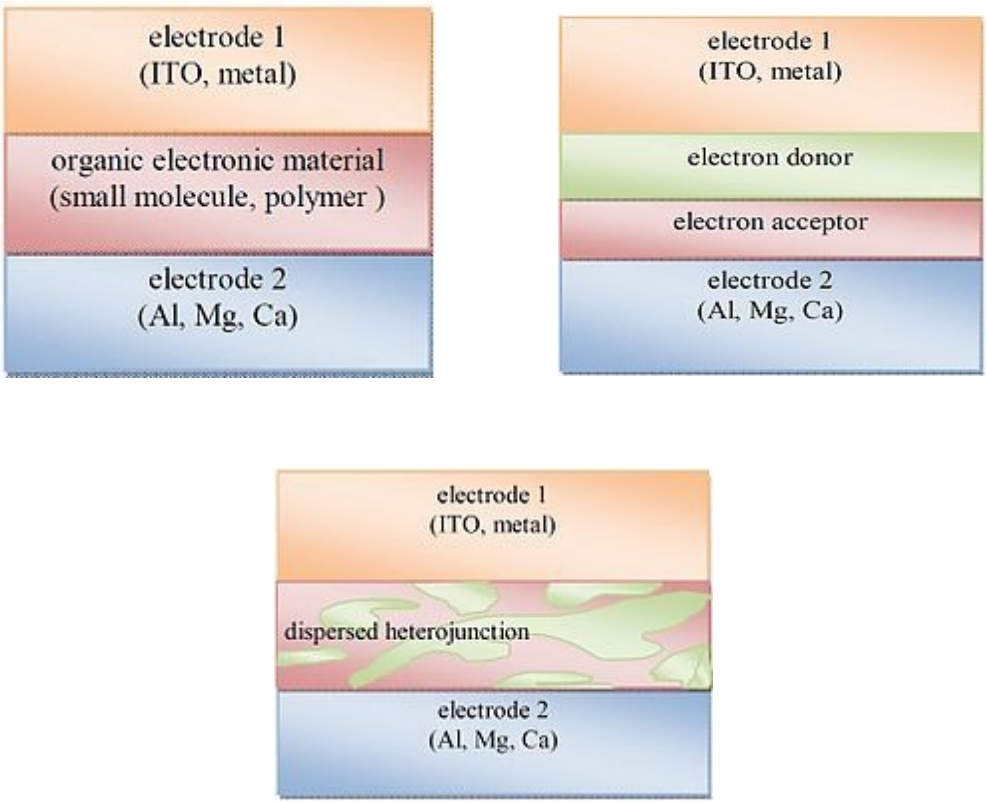

Fig2.1 :schematics of (a) single layer (b) bilayer, (c) dispersed heterojunction solar cells

In Dispersed heterojunction cells however, the electron donor and acceptor are mixed together to form a blended active layer. The electron acceptor helps dissociate the excitons by attracting the electrons from the polymer to itself so that recombination is impossible. The holes left behind in the polymer then drift to the anode where oxidation takes place and the electron is transported to the cathode. The main criteria for the dissociation is that the electron affinity of the acceptor is larger than the ionisation potential of the donor.

In 1979, Tang filed a patent on his ability to increase PCE to 1% of a bi-layer PV device consisting of copper PC and a perylene derivative, and published his results in 1986. He proposed that the observed synergistic effect of bringing two different semiconductors in contact was caused by the field at the heterojunction interface. This local field he claimed aids dissociation of excitons diffusing to the interface.[25,29]

Hiramoto(1991) reported the first dye/dye-dispersed heterojunction in 1991. Using the same class of p- and n-type organic semiconductors as Tang, metal-free phthalocyanine (H2Pc) and a perylene tetracarboxylic derivative, he investigated the effect of introducing a third organic layer in the middle of a two-layer heterojunction PV. This middle layer was a mixture of the two dyes made by

co- sublimation from different thermal sources. He discovered that by introducing this third layer, the photo-current doubled as compared to the two-layered cell. [25,30]

The first report of a conducting polymer/C_{60} cell was in by Sariciftci et al(1993). Fullerene was vacuum sublimed onto a MEH–PPV layer that was spin coated on ITO-covered glass. Au was used as the electron-collecting electrode and a 2000% increase in photo-current was observed when C60 was added as a second layer, indicating that fullerene strongly assisted charge separation.[25,31]

Schmidt-Mende et al.(2001) fabricated PV cells of self-organized discotic liquid crystals of hexaphenyl-substitued hexabenzocoronene (HBC) and perylene. The perylene and HBC p-systems segregated into vertical rods, ideal for efficient charge transport. Using a 60:40 HBC:perylene blend, sandwiched between ITO and Au electrodes they recorded a peak QE of 34% and a PCE of 2% (at 490 nm). This ranks the cell among the best of the present day non-fullerene organic PV cells. [25,32]

Yu et al.(1994) made the first dispersed polymer heterojunction PV cell by spin-coating a solution of MEH-PPV and C60 in a 10:1 wt- ratio on ITO using Ca as the cathode. The device gave a photosensitivity of 5.5 mA/W, an order of magnitude higher than that of the pure polymer. In 1996 Kohler also used the same approach for fabricating PV and achieved good results.[25,33]

One limitation of this approach is the relative low solubility of fullerenes in normal solvents. This problem was solved when Hummelen et al. (1995) synthesised a number C60-derivatives with increased solubility which allowed the fullerene content to be as high as 80% in the prepared films. Using a methano-functionalised fullerene derivative, Yu et al. repeated the fabrication procedure with a polymer/fullerene ratio of 20/80, between ITO and Ca electrodes and produced a device with QE of 29% and a PCE of 2.9% (under a 20mW/cm^2 monochromatic light).[25,34]

Besides PPV derivatives, polythiophenes have been used in fullerene bulk heterojunction cells. Brabec et al(2003) showed that very high QE (76%) in P3HT/methanofullerenes bulk heterojunctions are attainable.[35] The limitation seems to be optical loss in the cell, thus QE approaching 100% should be within reach. Geens et al. have shown that sandblasting of the glass substrate can effectively reduce optical loss due to reflection in organic PV cells.[25,36]

The first reports of polymer/polymer bulk heterojunction PV came independently from Yu et al. and

Halls et al. (1995). Both worked with the same PPV- based derivatives: CN-PPV as acceptor and MEH-PPV as the donor polymer. Halls made a PV cell from a blend of the two polymers in equal amounts by spincoating. ITO and Al were used as electrode materials, and the organic layer was 100 nm thick. The cells had a peak monochromatic QE of 6% and peak monochromatic PCE of 1%. This type of composite cell was found to be three orders of magnitude more efficient than pure cyano-PPV (CN-PPV) and two orders of magnitude more effective than pure MEH-PPV. The effectiveness of this type of polymer-blend is strongly dependent on the morphology. Ideally the microphase domains should be no larger than the exciton diffusion length, which for PPV-type polymers is around 7 nm according to Halls. In addition the network should be bicontinuous, leaving a free path for both holes and electrons so that they can reach the respective electrodes without the necessity for tunnelling through domains.[25,37,38]

2.2 PCBM-P3HT

Poly(3-hexylthiophene)-[6,6]-phenylC61-butyric acid methyl ester is the conjugated polymer used as the bulk heterojunction in this project. Being the most efficient organic solar cell material thus far recorded[18], with an efficiency of ~5%[11,] it has been widely studied[11].

PCBM is a fullerene derivative soluble in chlorobenzene and due to its high hole mobility, it plays the role of an electron acceptor whereas the donor P3HT belongs to the polythiophene family. It is the excitation of the pi orbit electrons in P3HT that gives the PV effect in the blend.

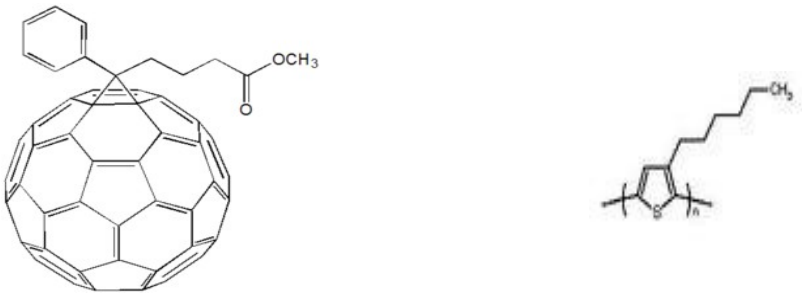

Fig 2.2: a) molecular structure of PCBM b)molecular structure of P3HT.

2.2.1 BANDGAP AND EFFICIENCY

It's bandgap is about 1.8eV so that the largest absorption wavelength is about650nm. A unique feature of polymers is that their band gap are readily altered even without a change in chemical composition. It has been shown, that the alignment of the P3HT can alter the band gap of the blend significantly. Generally, a head-tail alignment of P3HT has a narrower bandgap than a Head-Head

alignment. In addition, the ratio of P3HT:PCBM may significantly alter it too[18].

The efficiency of PCBM:P3HT can be increased by giving it a more organized morphology. Experiments have shown that such blends result in a widened absorption spectra, an increased J_{sc} , a decrease in surface resistivity and a slight decrease in $V_{oc.}$ This can be achieved through annealing.[18] Experiments have shown that after annealing, P3HT form long and thin fibres while PCBM crystals become more homogeneous thus giving the blend a more organized structure.

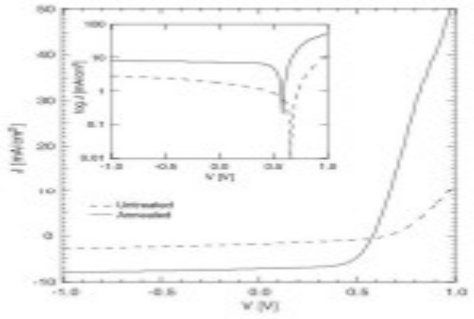

Fig 2.3: A typical I-V curve of P3HT:PCBM blends before and after annealing .[18]

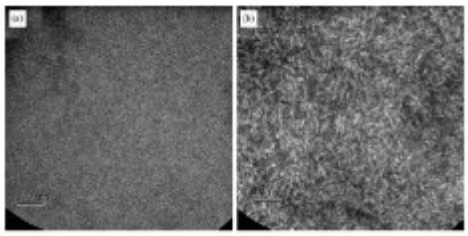

Fig 2.4: TEM images of a P3HT:PCBM 1:1 blend (a) before and (b) after annealing at 100 °C for 5 mins

Other means of achieving this are dye introduction, to increase near IR region photoconversion, introduction of hole extraction layer such as PEDOT:PSS, etc.

2.2 .2 STABILITY

PCBM:P3HT is relatively stable compared to other active polymer layers. Experiments have shown that under accelerated light soaking conditions in the laboratory, it remains good even after a year of outdoor exposure.

PCBM:P3HT ratio, morphology and the cathode material also affect stability. For instance a Ca/Ag cathode semiconductor retains a sufficiency for a significantly longer time than a LiF/Al cathode[18].

2.3 ADHESION AND CHARGE TRANSPORT

The efficiency and stability of the cell depends largely on the charge transport both within and outside the active layer. If this charge transport is high, these will also be high and vice versa. For very rough layers, the adhesion between layers at the interfaces will not be too good and this tends to slow down the rate of charge transport across layers.

The delamination between layers of OPV devices during charge transport and other nouvel fabrication methods have resulted in the need for better understanding of adhesion between layers.[21] Several adhesion theories exist and although methods such as contact angle measurements, scratch or peel tests etc have been used in adhesion measurements, they still have not provided nanoscale measurements for adhesion.

2.3.1 ADHESION THEORIES.

Adhesion is the tendency of dissimilar surfaces to cling to one another due to bonding at the atomic scale. There have been several attempts at comprehensively explaining the adhesion phenomenon but a generalized theory is still yet to be derived as most theories are unique to particular systems.[39,40] In formulating these theories, five different mechanisms are considered: mechanical, adsorption, chemical, diffusion and electrostatic. [39,40]

Mechanical adhesion involves the interlocking of a solidified adhesive with the roughness and irregularities(crevices, cracks, pores etc) of the surface of the adherent and it plays a very vital role at the microscopic scale.[40] The adhesive penetrates these features and hardens such that it keys into the surfaces and forms a strong surface bond. It is thus able to bond two surfaces together and ideally the only weakest part of the bonded joint is the adhesive strength.

Adsorption mechanisms depend on secondary bonds(Van der Waal's forces) between the adhesive and the adherent. [39,40] Here, the only requirement is that materials are brought close enough or in contact so that a bonding process is activated.[39,40] as they occur as a result of the presence of nuclei and electrons. Although these forces are comparatively small, they are large enough, to make resulting attractions considerably greater than any observed strengths .[40]

Diffusion theories involve the diffusion of the macromolecules of the adhesive into the substrate or the interpenetration of the molecules of each material removing the interface between them.[40] It is

very common in polymers.[40]

Electrostatic adhesion mechanism is as a result of the electrical double layer existing at the interface between the metallic electrodes and the polymer and unlike others, the force here is independent of the separation. [40]

Chemical theories involve, both primary and secondary chemical bond contributing to adhesive bond strength.[40] These bonds may be covalent or ionic character. Surface characterization and some analytical methods, have brought this into limelight in recent times and have revealed fragments of bonding compounds within fractured surfaces of broken bonds.

Different models exist based on varying material and geometric properties of interacting layers such as The Derjaguin-Muller-Toporov (DMT) model applying to weak interactions between stiff materials with small radii; The Johnson-Kendall-Robert (JKR) model which considers strong interactions between compliant materials with large radii; and the Maugis-Dugdale (MD) model which lies between the DMT and JKR models. These models continue to form the basis for obtaining the adhesion energies from adhesion forces today.[40]

2.3.2 AFM THEORY AND PULL OFF

A very recent technique which is still being investigated on OPVs is the AFM technique. It is an imaging technique that typically maps a surface with respect to surface topography. By coating AFM tips with complimentary materials, pairwise interactions between layers relevant for modelling organic electronic structures are measured.[21] An effective understanding of the various layers of the OPV by this technique has a great potential of enhancing the understanding of the dendrite formation, and consequently improving device stability and efficiency. This is because, although it covers only a limited analysis area, it has an excellent lateral and height resolutions (angstroms range), which make it the very good for studies of morphological changes on a nanoscale.

First, the micro-fabricated cantilever probe is attached to a scanner head which is lowered at a constant velocity to the surface. As it is lowered down, it is pulled into contact with the surface by adhesive force interactions between the surface and the probe tip.[21]

The scanner continues its downward motion with the substrate and probe in continuous contact causing the tip to bend under elastic deformation. When the tip direction is reversed, the scanner head is lifted and the tip elastic deformation is reversed while the residual adhesive force prevents the tip from detaching off the surface at zero load hence the reverse loading is continued until the forces are eventually overcome. This negative load corresponds to the pull-off force and is related to the displacement deflection, via Hookes law.[21]

It has been used to study microscopic holes in the outer electrode of OPV devices and which showed that each microscopic hole was centred in a surface protrusion. The microscopic holes were found to be the main entrance channels for oxygen and water while the protrusions were suggested to be a consequence of the resulting oxidation of the underlying organic material due to the formation of oxides. It has also been used in studying adhesion between layers where it was discovered that organic-organic interfaces adhere more than the inorganic-inorganic ones[21].

2.3.3 ADHESION ENERGY MODELLING AND INTERFACIAL FRACTURE MECHANICS

The adhesion energy corresponds to the mode I energy, G from a fracture mechanics point of view. For crack growth between two surfaces of energies 1 and 2, the adhesion energy will be

$$G_{adh} \sim G_{elastic} = \gamma_{surface\ 1} + \gamma_{surface\ 2} - \gamma_{surface\ 1\text{-}2}$$

as already stated above,various adhesion models exist based on the different material and geometric properties out of which three are considered here.

1. **The Derjaguin-Muller Toporov(DMT) model**

This is used for characterising weak interactions between stiff materials with small radii. Here, adhesion energy is related to the force by

$$V_{dmt} = F_{ad}/2\pi R$$

2. **Johnson-Kendall Robert(JKR) model**

This is used for strong adhesive forces between materials with large radii. Here the relationship between the force and energy is given by:

$$\gamma_{JKR} = 2F_{ad}/3\pi R$$

3. **The Maugis-Dugdale(MD) model**

This lies between the DMK and the JKR model and involves the use of analytical methods in

getting a relationship between the adhesion force and energy. An iterative method has been developed by Capick et al, Pietrement, and Troyon[41,42] which gives an approximation of the MD adhesion energy to within 1% accuracy. A good knowledge of the combination of material and geometrical properties is used to characterise the range of adhesion model by calculating a non-dimensional parameter λ.

$$\lambda = 2\sigma_o(R/\pi K^2\gamma)^{1/3} = -0.913\ln(1-1.1018\alpha)$$

where R= effective radius given by

$$R = (1/R_{tip} + 1/R_{rms})^{-1}$$

and K is a constant given by

$$K = 4/3[(1-V_1^2)/E_1 + (1-V_2)/E_2]^{-1}$$

σ_o = constant adhesive force between both bodies(non zero at small distances).

$$\gamma = G/2 = F_{ad}/\pi R F_{ad}$$

where $F_{ad} = 0.267\alpha^{2-} 0.767\alpha + 2$

Values of $\lambda < 0.1$, $\lambda > 5$ and $0.1 < \lambda < 5$ correspond to the DMT, JKR and MD models respectively. Conversion of pull off forces to measurements of adhesion energies over a wide range of scenarios are thus made possible with the above expressions.

2.4 DEGRADATION

Unlike inorganic solar cells, organic ones are unstable under illumination and in the dark because they readily degrade. However for real life applications, cells with long life and stability are required hence the need for a proper understanding of the degradation mechanisms and methods for reducing them. Various research works at the moment are focussed on the search for better active materials, improvement of active layer processing, encapsulation mechanism, application of getter materials and UV fillers, etc in order to tackle this.[44] There are two major modes of degradation-chemical and physical.

The chemical degradation results are due to oxygen, water, polymer and electrode reactions with one another or with the active layer. Oxygen is readily activated during UV illumination forming super oxides and H_2O_2. wich then attack polymer substances present. PPV type polymers are particularly prone to this and degrade in a matter of minutes under 1000Wm^{-2} illumination. P3HT

cells are more stable though also susceptible to it.

Degradation is also a function of polymer preparation. The procedure of preparation is bound to affect the device performance. The concentration of solution, purity of the polymers, type of solvent, ratio of polymer(for multiple polymers in blends) etc are all factors that are actually being researched upon to bring about an optmized preparation procedure.[43]

Thus far, the optimal ratio of P3HT:PCBM in blends is 1:0.7 while the optimal solvent according to Yanfei Ding et al.[43] is dichlorobenzene as against chlorobenzene(used in this work) and chloroform based on their work on "Optimizing material properties of BHJ polymer films for PV applications".

The spatial organization of the different materials into layers with a precise thickness tailored for optimum photon harvesting and charge-carrier transport is the basis for physical and mechanical degradation in organic solar cells. In the bulk heterojunction cells, a further requirement is the nanophase separation of the active layer into an interpenetrating network of donor and acceptor material. Obtaining an optimal structure/morphology have been at the center of OPV researches for a while now. This structure is not static after device fabrication as small organic molecules like PCBM and even P3HT still have some freedom to diffuse slowly or recrystallize over time especially at elevated temperature.

These gradual changes in the microstructure will lead to a degradation of the performance of the OPVs. This type of physical degradation is harder to study because we need methods to map the internal three-dimensional (3D) structure and to correlate this with device performance. Different types of microscopy have been used to gain insight into the size distribution of PCBM crystallites as a function of heat treatments (annealing).

In studying the phase segregation of MDMO-PPV/PCBM active layers, Yang et al.[44] found that the PCBM aggregates formed microcrystallites which grew larger with time. The effects of thermal ageing were also studied [44]. Annealing was observed to increase short circuit current. They linked the morphology changes to the rather low glass-transition temperature (Tg) of MDMO-PPV and also noted that higher-Tg materials such as P3HT might increase device stabilities. Kline et al. used a combination of AFM and X-ray diffraction techniques to investigate the effect of polymer molecular weight of P3HT on morphology. Small molecular weight P3HT formed a mesh of rod-like structures while high molecular weight P3HT was more homogeneous.

The more ordered small molecular weight P3HT had a lower hole mobility explained by trapping of the carriers in the ordered domains that were poorly connected. Similar fibril-like P3HT crystallites were observed by Klimov et al. [45]and by Yang et al.[46] in P3HT/PCBM mixtures from which they concluded that annealing devices at 120°C resulted in a stable morphology with device lifetime in excess of 4days at 70°C under sun illumination [46]. Enhanced thermal stability of the morphology and hence the device performance have been reported for a variation of P3HT co-polymerized with a small amount (~4 mole%) 3,4-dihexyl-thiophene [47]. The dialkyl monomer introduces a slight disorder and lowers the regio-regularity of the material. Devices made from this copolymer formed stable nanophase separated bulk heterojunction structures on short-time annealing (30 min, 150°C) as observed by transmission electron microscopy. The authors thus suggested that the high device efficiencies obtained with commercial P3HT of 5% may be due to a fortuitous lower regio-regularity.

2.4.1 DEGRADATION MEASUREMENTS

The table below lists useful and relevant techniques for studying degradation mechanisms in OPVs, and, in addition, lists relevant information associated with each method.

*Table 2.1: Showing various techniques for studying degradation mechanisms in OPVs.*44

Useful and relevant techniques for studying degradation mechanisms in OPVs and relevant information

Technique	Bulk analysis	Surface analysis	2D imaging	Depth profiling	Destructive analysis	Non-destructive analysis	Chemical information	Morphological information
IV-curves	•					•		
IPCE (EQE) measurements	•					•		
Impedance spectroscopy	•					•	(•)	(•)
UV–vis spectroscopy	•				(•)	•	•	(•)
IR spectroscopy	•				(•)	•	•	
X-ray reflectometry	•				(•)	(•)		•
RBS	•				•	(•)	•	(•)
TOF-SIMS		•	•	•	•		•	(•)
XPS		•	•	•	•		•	(•)
AFM		•	•		•		(•)	•
SEM		•	•		•			•
Interference microscopy		•	•		•			•
Efficiency 2D-imaging	•		•			•	(•)	(•)
Fluorescence microscopy	•		•		•		•	
Spectroscopic ellipsometry	(•)			(•)		•	(•)	•

However, two of these are considered in this work -IV and AFM measurements discussed below and in section 2.4.2 respectively.

J-V measurements are the most detailed source of information on degradation. From the evolution of the J-V-curves information on J_{sc}, V_{oc}, FF, PCE, R_{sh}, R_s can be extracted and the general shape of the curve can be used to follow the degradation of the device performance. The maximum short circuit current, open circuit voltage, Fill Factor or power conversion efficiency (J_{sc}, V_{oc}, FF and PCE) are measured as a function of time. Of these, the most useful are Jsc and PCE as they directly tell of the device operation and reflect best how it degrades. The Voc also degrades as a function of device lifetime but is not always as straightforward as it is not linked to the machinery of the cell in the same way as the Jsc and PCE that both reflect the ability of the device to convert photons into electrons or energy.

A curve of any of the chosen parameter as a function of time shows a picture of the degradation. The shape may take may be linear or exponential, depending on the dominant degradation mechanism and from it half-life times can be calculated.

The purpose of measuring the lifetime of a device through a decay curve has several purposes. Firstly, it establishes qualitatively whether the particular device is stable and how it degrades. Secondly and more importantly, it allows for the comparison with devices prepared from different materials and or under different conditions thus ideally provide a method for improving polymer solar cell stability through design of materials, devices and fabrication methods amidst other purposes.

2.5 ELECTRON AND HOLE TRANSPORTING LAYERS.

In this project, poly(3,4-ethylenedioxythiophene)poly(styrenesulfonate)(PEDOT:PSS) was used as a hole transporting layer in all cases while no electron transporting layer was used. It is an optically transparent, conductive and ductile polymer comprising of PEDOT and PSS ionomers. It performs three main functions in the device.

(i) it acts as a selection layer through which the holes from the active layer to the anode are transmitted and the electrons are reflected back.
(ii) it helps to laminate and smoothen the ITO surface to prevent short circuiting.
(iii) It has a higher work function than the ITO so that it gives a better alignment of the

work function with the HOMO level of the active layer.

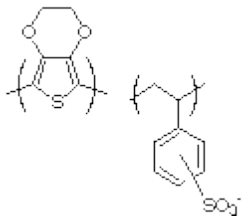

Fig 2.5: molecular structure of PEDOT:PSS.

2.6 THE ELECTRODES

The cathode material used for this work is aluminium. Deposited by evaporation, other possible materials that can be used are calcium, magnesium, magnesium/indium etc.[28] They have a relatively low work functions, necessary for the setting up the field in the device.

ITO with its high work function is the most widely used anode in PV devices.[25] It is a solid solution of Indium III oxide(In_2O_3) and Tin IV oxide(SnO_2) 90%:10% by weight. It is optically transparent, colourless and has a high electrical conductivity. However, ITO- polymer surfaces are not well understood hence they cannot be effectively controlled in organic photovoltaic applications. Large variations in ITO morphology and work functions have been observed from various studies. The general non uniformity of ITO surfaces generally contributes to rapid polymer degradation despite their being annealed after deposition. Also, oxygen and indium atoms may diffuse into organic layers, sometimes reacting with them to yeild undesired effects. A way of reducing this effect is by introducing a hole transporting layer, generally PEDOT:PSS.

2.7 THIN FILMS

These are layers of materials ranging from fractions of a nanometre(monolayer) to several microns in thickness. Several methods of depositing thin films exist and in this work, sputtering, spin-coating and vacuum evaporation are used.

2.7.1 SPUTTERING

This is a PVD method of depositing thin films by ejecting materials from a target to a substrate such as glass with the aid of strong magnetic and electric fields. It takes place in a vacuum chamber brought about by mechanical and vacuum pump system. A substrate(to be coated) is placed at a

distance above a target (containing the material to be deposited). An electric field is then set up between them both while simultaneously allowing some Argon gas into the system. This electric field ionises the gas such that is then attracted to the target cathode(negatively charged) and it consequently sputters the atoms in the target material which eventually settle on the substrate.

It is what is used in depositing the ITO thin film used as the anode in this work. Various types of sputtering systems such as facing target sputtering system and RF sputtering systems exist and have been used in depositing ITO for solar cells in the past. For very good film quality, four factors are of importance viz sputtering rate, temperature, sputtering pressure and sputtering gas mixture[16].

In studying the effects of vacuum level on film properties,Kana et al(2005) used a 13.56MHz radio frequency magnetron sputtering system (same as used in this work) with a 40W rf power system, 6.7E-7 to 6.7 E-5 hPa. 2.1Pa Argon pressure, and 3.5cm target substrate distance, in depositing 80nm thick ITO on different substrates[16]

2.7.2 SPIN-COATING

Apart from blade coating, which is seldom used, the most popular technique used in depositing active and conducting layers for OSC and HSC is spincoating. It entails spreading a solution on a substrate by rotation at very high speeds. It is usually done by a spincoater(also used for etching and cleaning). For very thin films, the angular speed should be very high as most solvents are volatile and evaporate simultaneously. The angular speed, rotation time, and solvent density are factors that influence the resultant thickness of any film.

2.7.3 THERMAL EVAPORATION

Vacuum evaporation is a deposition method whereby a source material is evaporated in a vacuum. The vacuum allows vapour particles to travel directly to the target object where they condense back to solid state. An evaporation system includes a vacuum pump and an energy source which evaporates the material for deposition. Thermal evaporation is used in this work although, several energy sources exist.

The purity of the deposited film is a function of the vacuum quality and source material purity whereas its thickness varies with the geometry of the evaporation chamber. Cathodic deposition for most OSCs are ~5E-6 mbar[11,23].

EXPERIMENTAL PROCEDURE AND DISCUSSIONS

The experiment aimed at comparing the degradation features in different OPVs fabricated under different conditions hence it involved the optical, electrical characterisation and morphological studies(including adhesion studies) of both the several devices fabricated and also some semi-devices.

Materials used during the process included Aluminium masks, corning glass slides of 1.2mm thickness, poly(3-hexylthiophene-2,5-diyl)(P3HT)powder, [6,6]-Phenyl C61-butyric acid methyl Ester(PCBM) powder, chlorobenzene, PEDOT:PSS solution, Aluminium foils, Indium tin oxide, a sputtering machine, a thermal evaporator, a spin-coater, an ultrasonic cleaner, a glove box, a nitrogen gun, a stirrer, deionised water, acetone, ethanol, a surface profiler, a scanning electron microscope, an EXRF spectrometer, a spectrophotometer, a four-point probe etc.
In fabricating the device above, five major steps were carried out- mask fabrication, substrate preparation, active layer preparation, thin film depositions and finally characterisation.

3.1 MASK FABRICATION

The masks were used in providing the required geometry for each layer. Two sets of masks were used in this study, each set being used for the deposition of the two different electrodes. The electrodes were masked in such a way as to avoid short-circuiting. For the ITO masks, three equally spaced 1.5*1 sq. cm rectangular boxes were cut out of a 7.5*3.0 sq. cm aluminium sheets using a laser cutter. The same was done for the Aluminium cathode but with a dimension of 1*1sq.cm. They were then filed and cleaned. The cleaning was done, first by washing with decom 90 and deionised water after which they were then placed in a 230V VWR ultrasonic cleaner(Fig 1) for 10 minutes at 40^{O}C, dried with a nitrogen gun and stored in a desiccator, pending usage.

Fig 3.1: Materials used for cleaning. a)The ultrasonic cleaner. b) the nitrogen gun

3.2 SUBSTRATE PREPARATION

The substrates used for the devices here were 7.5*2.5 sq. cm corning lime glass slides. First they were cut into three equal parts with the aid of a pen, ruler and a PMT-059 diamond cutter. About 30 of these were then placed in a sample holder, then washed using decom 90 and deionised water before being placed in a beaker of acetone and then into the ultrasonic cleanser for the same conditions as the masks. They were then dried using a nitrogen gun(Fig 3.1b) after which they were placed in a sample holder and then left in a desiccator.

3.3 ACTIVE LAYER PREPARATION

The active layer used is a blend of poly(3-hexylthiophene-2,5-diyl), regioregular, electronic grade manufactured by Sigma-Aldrich Co., USA and [6,6]-Phenyl C61-butyric Acid methyl Ester(PCBM) a fullerene derivative manufactured by American Dye Source, Inc., Quebec.

Fig 3.2: Active layer materials used, stored in amber bottles.

First, the beakers, conical flasks, magnetic ball(used for stirring) were subjected to necessary cleaning conditions, after which three attempts aimed at preparing the active layer were embarked upon.

For the first, 56mg of P3HT and 57mg of PCBM were each separately weighed out using an Ainsworth DE-100 weighing balance and then dissolved in a 10ml of J.T. Baker chlorobenzene to make two approximately 6mg/ml solution. These were then separately stirred at 50^{O}C each on a 500W Jenway model 1000 stirrer for thirty minutes each, to dissolve them, after which both solutions were mixed and stirred together in a fairly covered beaker at uncontrolled temperature. After about 24 hours, the entire solvent was discovered to have evaporated.

The process was then repeated, but this time around a well sealed conical flask rather than a beaker was used for the experiment and a controlled temperature of about 80^{o}C. A 60mg of PCBM and a 58mg of P3HT were dissolved to give an approximately 10mg/ml solution. An excess of 3ml solvent was then added to provide for solvent evaporation while also covering the entire system with a carton. This was used in fabricating the first sets of devices(Specimen 1).
For the third attempt, an exactly 20mg/ml solution was prepared and stirred at room temperature for 24 hours under the same conditions as above. This solution was then used to make the second set of devices(Specimen 2).

Fig 3.3 : a) the active layer being prepared on the stirrer. b) the set-up covered by a carton to minimise vaporisation.

In the later two cases, the solution was filtered using a whatman filter paper of 11μm particle retention before they were eventually used in fabrication.

3.4 THIN FILM DEPOSITIONS

Fig. 3.4 shows the general structure of the OPV device fabricated. Each thin film layer was deposited bottom up, one upon the other with different techniques discussed below.

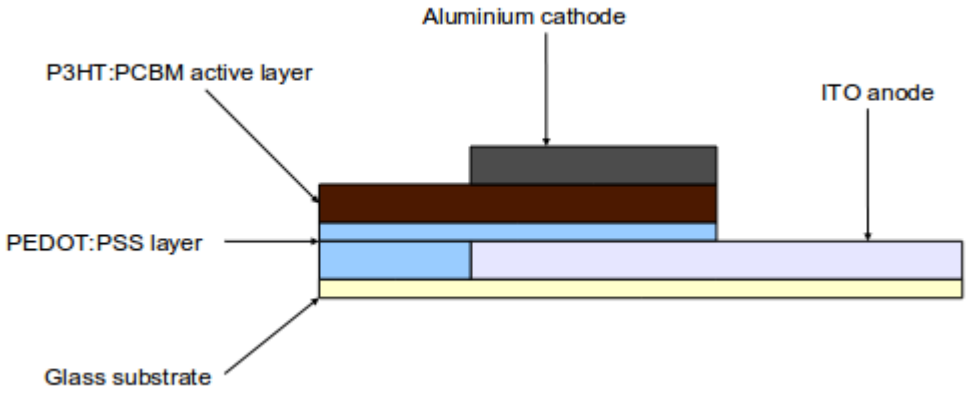

Fig: 3.4: Side view of the P3HT:PCBM solar cell fabricated

3.4.1 ITO DEPOSITION

An Edwards FL 400 13.56MHz radio frequency(RF) magnetron sputtering system was used for all ITO depositions. First, the 99.99% In2O3:SnO2 ceramic target surface was cleaned by pre-sputtering for ten minutes after which two sets of nine glass substrates each were placed upon the aluminium masks already placed on a sample holder. The sample holder was then fit into the sputtering chamber. With an Ar flow rate of 0.8SCCM, an RF power of 40W, an approximately 100nm thick ITO layer was deposited on the substrate after 65minutes. The deposition rate was 0.17^{0}A/s while the system pressure ranged between $7*10^{-3}$ to $3.2*10^{-3}$ for a substrate target distance of 6cm. After sputtering, the substrates were then annealed in a carbolite furnace at 250^{o}C for 60minutes to decrease the sheet resistance and improve the long-range order crystalline quality of the ITO. The annealed ITO coated substrates were then stored in a desiccator while the active layer was being prepared.

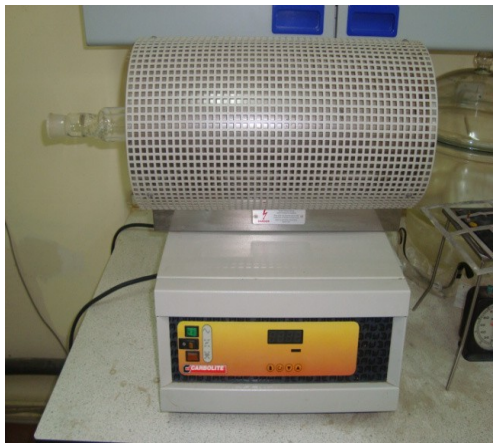

Fig3.5 a) the sputtering system used b)sputtering chamber of the system c) the carbolite furnace used for annealing.

3.4.2 PEDOT:PSS DEPOSITION

All PEDOT:PSS depositions were done using a WS 650Hz model laurell spin-coater. First, the spin-coater was switched on and programmed. Then some Nitrogen gas was passed into the spin-coating chamber. All ITO coated glasses were first masked in such a way that an area of 0.5cm^2 of the ITO was covered by a masking tape to protect an area which was later on to be used as a contact. The PEDOT:PSS solution bought from H.C. Stack Inc. USA was filtered using a filter paper to remove all undissolved particles. An already pre-cleaned hypodermic, sterile, non-toxic and pyrogen free 5ml syringe was then used in measuring out some quantity after which 0.4ml was statically dispensed unto the substrate already placed on the spin-coater. The substrates were spun in three stages. The first helped spread the pedot:pss for 5seconds at a speed of 500rpm and acceleration of 100rpm/s, the second, an intermediate step was 1500rpm, 1000rpm/s for 3 seconds while the final

aimed at thinning the layer was for 60s at 3000rpm and 1500rpm/s. After an aggregate of 68s it was they removed and baked for 15minutes at 100^{O}C using the same carbolite furnace as above and stored in a rack pending when the active layer was ready.

*Fig 3.6: Showing the spincoating chamber and the controller**

3.4.3 P3HT:PCBM DEPOSITIONS

All depositions were done using the same laurell spincoater as above. Here it was programmed into two stages with speed, acceleration and rotation time of 400rpm, 255rpm/s, 10s and 800rpm, 1105rpm/s,30s respectively. 0.3ml of the already pre-filtered solution were statically dispensed using the same syringe types as above after which the process was started and eventually terminated after 40seconds. Again, they were then dried using a hot plate for 15 minutes at 140^{o}C.

3.4.4 ALUMINIUM DEPOSITIONS

All Aluminium depositions were done using an Edwards FL 400 thermal evaporator and the 1cm*1cm masks. A small mass of aluminium is placed in the filament, where it is heated up and using a pressure of $2.0*10^{-5}$, and an Argon flow rate of 0.8SCCM, the thickness of aluminium recorded on the deposition controller was 200nm.

Fig 3.7a) the thermal evaporator used for the aluminium deposition. b) the evaporating chamber showing the substrate holder and filament.

3.4.5 ATOMIC FORCE MICROSCOPE TIP PREPARATION

Two atomic force tips to be used for adhesion studies of some of the layers deposited on plain glass were also coated with Indium tin oxide. These are to be used for the second part of this work to enhance the understanding of charge transport mechanism between layers. This coating was done using the sputtering system above and under the same sputtering conditions. They were also annealed under the same time and heat condition as above and then kept in a desiccator.

3.5 OPTICAL AND ELECTRICAL CHARACTERISATION

Several characterisation processes were carried out on both the main device and semi-devices(various layers or layer combinations deposited on glass) and these are discussed below.

3.5.1 THICKNESS AND ROUGHNESS DETERMINATION

The thickness and roughness values were measured using a Veeco dektak stylus profiler. It uses a diamond tipped stylus of radius 12.5um to detect minute surface variations in the surface topography. The stylus is mechanically coupled to the core of a linear variable differential transformer.(LVDT). A precision stage moves the sample surface across an optically flat reference surface beneath the stylus. As the sample is moved by the stage, the stylus rides over the surface detecting roughness variations as small as 1nm in height with an impact force of 3mg. The LVDT generates an analogue signal corresponding to the vertical stylus movement. The signal is then

amplified, conditioned, digitized and stored for manipulation, analysis and display.
In determining the roughness for all specimen analysed, a high(short) and low(long) pass cut off filter of 1/100 and 1/10 of the scan length respectively was used. The later is used to calculate waviness data while the former is used for roughness data. Scan lengths used were between 1000 and 4000um. After scans, the profile is levelled on the screen and then, the average roughness values which is the arithmetic mean of the departures of the profile from the mean line is read from the bottom left side of the screen.

Fig 3.8: a) the Veeco surface profiler used b)the interior of the profiler

For thickness, measurements, the specimen were made in such a way that a portion was film free either by scratching, drawing lines or wiping a region so that the stylus was made to scan through both regions and then the thicknesses could be derived relative to the other.

3.5.2 TRANSMITTANCE AND ABSORPTANCE MEASUREMENTS

A spectrophotometer was used in measuring the transmittances of each layers. The absorption were determined using the conservation of light equation

Incident light(I) = Reflected beam(R) +transmitted beam(T) + absorbed beam(A).

Assuming a zero reflectance,

$$I = T + A \quad => \quad A = 1 - T$$

The characterisation set up consists of a light generating source, the sample holder, a detector, input and output optical fibres and a software built within a system. For all characterisations, the

spectrophotometer software was first turned on, then the spectrophotometer. The zoom range for the measurement was set to wavelength 200-900nm(which is the wavelength range for visible light) on the x-axis and transmission 0-100% on the y-axis. The spectrum when no specimen is placed in the system was then observed and set to 100% so that every other measurements were taken relative to air. Each specimen were then placed one after the other on the sample holder and the light source was turned on. The transmission data appearing on the screen and was then saved to a file. The process was then repeated twice to confirm that the first results were accurate.

3.5.3 SHEET RESISTANCE DETERMINATION

The sheet resistances of layers were determined using a four point probe. It is a machine which can be used in determining film thicknesses, sheet resistances and bulk resistivities. Its schematic is shown in fig 3.9.

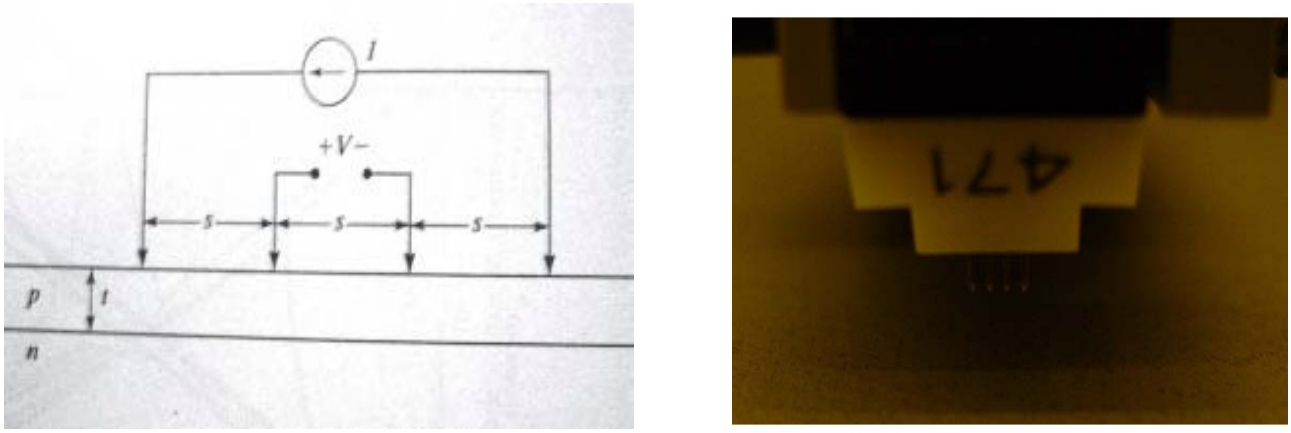

Fig 3.9: Four-point probe a)schematic b)actual

The theory behind it is that a fixed current is injected into the specimen through the outer probes and the voltage is measured between the two inner probes.
The resistivity ρ is given by

$$\rho = 2\pi sV/I\mu ohmcm \qquad \text{for } t>>s$$

where s=probe spacing ; V= measured voltage; I = Current and t= specimen thickness

$$\text{and} \qquad \rho = (\Pi t/\ln 2)V/I\mu ohmcm \qquad \text{for } t<<s$$

so that the sheet resistance can then be determined by the formulae

$$R_s = \rho/t = 4.53V/I$$

All specimen analysed for sheet resistances were probed at four different points and then the average V/I values were taken and used in computing the sheet resistances.

3.5.4 ELECTRICAL CHARACTERISATION OF THE DEVICE

All electrical characterisations of PV devices in this study were done using a model 4200-SCS keithley semiconductor characterisation system. It consists of a light source, and an electrical Source measure unit mounted on a computer system. It is a system that includes instruments for measuring both I-V and C-V characteristics and also possesses a software, graphics and mathematical capabilities.

First the device was mounted on a holder which exposed only its active area. It was then connected to one of the system's Source measure unit(SMU)whose schematic is shown below. A four wire connection is used such that a voltage is sourced across the PV cell using one pair of leads(Force Hi and Force Lo) and the voltage drop across the cell is measured across a second set of leads(Sense Hi and Sense Lo). For dark characteristics the light source was turned off but for light characteristics, a simulated AM1.5 irradiation from a solar simulator (Edwards) of intensity 100 mW cm^2 was used in taking measurements.

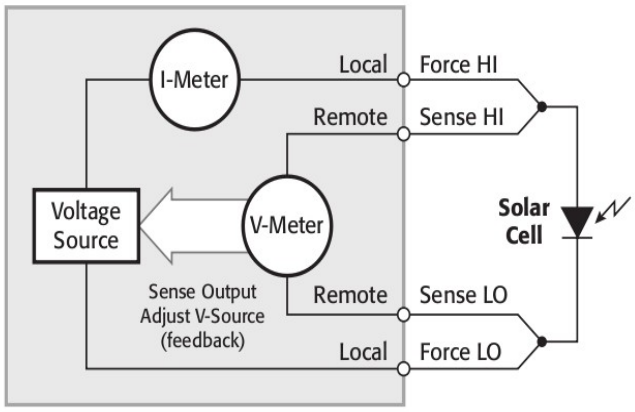

Fig 3.10: Schematic of the Source measure unit system used.

The sweep voltage, number of iterations and maximum current were then set on the software alongside the current density which was programmed to give the quotient of the measured current and the device active area after which the program was run. A typical plot of the dark and light characteristics curves expected to be observed are shown below. The light curve passes through the fourth quadrant because the system allows power to be extracted from the device(I-,V+)

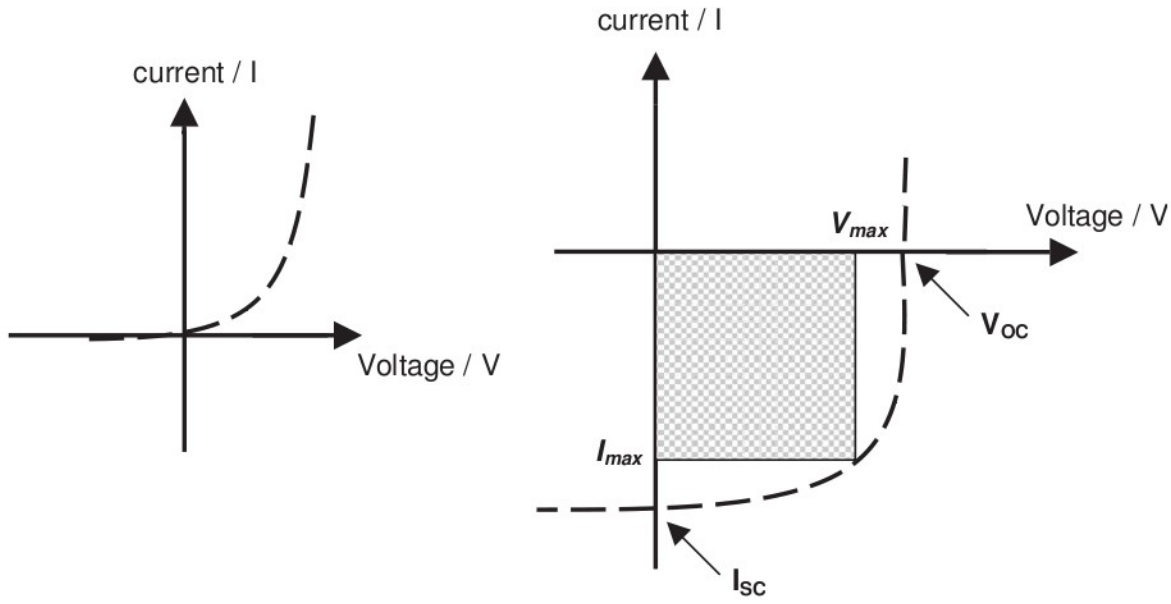

Fig 3.11 : Typical I-V curves for a solar cell a) in the dark b) under illumination

Forward bias J-V measurements are generated under controlled illumination by setting the SMU to a source voltage sweep and measuring the resulting currents and current densities iteratively. The voltage source is the open circuit voltage V_{oc} when the current is zero while the current is the short circuit current I_{sc} when the voltage source is zero. The parameters V_{oc} and I_{sc} can be derived from the sweep data using the model 4200=SCS built in mathematical analysis tool, the formulator or can be determined from the output graphs. The fill factor(a measure of how far the I-V characteristics of the cell differs from an ideal one and efficiency can then be calculated as

$$FF= I_{max}V_{max}/I_{sc}V_{oc}$$

$\eta = P_{max}/P_{in}$

where,

I_{max} = the current at the maximum power output

V_{max} = the voltage at the maximum power output

I_{sc} =the short circuit current

V_{oc} = the open circuit voltage

P_{max} = the maximum power output

P_{in} = the power input to the cell defined as the total radiant energy incident on the surface of the cell

Reverse bias measurements can be used in determining leakage current and shunt resistance. The test is typically done in the dark and the voltage is sourced from 0V to a voltage level where the device begins to break down. The resulting current is measured and plotted as a function of the voltage. The shunt resistance is given by the slope of the linear portion of the curve.

For degradation studies, the outputs, J_{sc}, V_{oc} , ŋ and FF are observed over regular intervals and are then plotted as a function of time. The half life time of the photovoltaic cell characteristics may also be determined too.

3.6.0 OBSERVATIONS ON VARIOUS SPECIMEN STUDIED

3.6.1 DEVICES

Specimen 1

ITO/PEDOT;PSS/P3HT;PCBM/Al

The SEM image of the top of the device surface initially, is shown below. Similar images are expected for all other devices. Traces of the adhesive tape used in masking were observed on the ITO contacts.

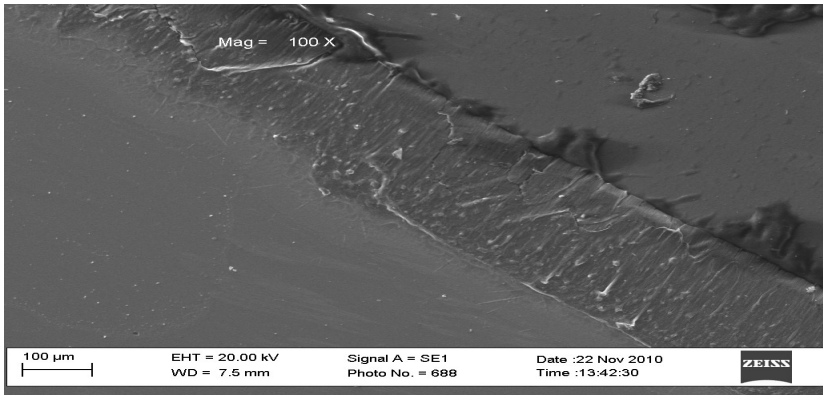

Fig 3.12: SEM image showing a portion of the device's top surface -the aluminiun(down left) and ITO(top right).

It's J-V characteristics were studied both under illumination and in the dark simultaneously. First the device was mounted and connected to the SMU, the current density set to the quotient of current and area(1sq.cm) on the software and the iteration set to 50. The forward bias was observed at times t= 0 and t= 10mins while the reverse bias was observed at time t=20s the sweep voltage used for times t= 0 and 20minutes was 0-6V while that for time t=10minutes was 2V.

Figure 3.13 shows the results obtained in the dark for the device. A plot of current density(A/cm^2) as a function voltage(V), it shows a working device albeit an ohmic one rather than a diodic device as current density is approximately directly proportional to voltage in all three cases. All three curves were also observed to be similar.

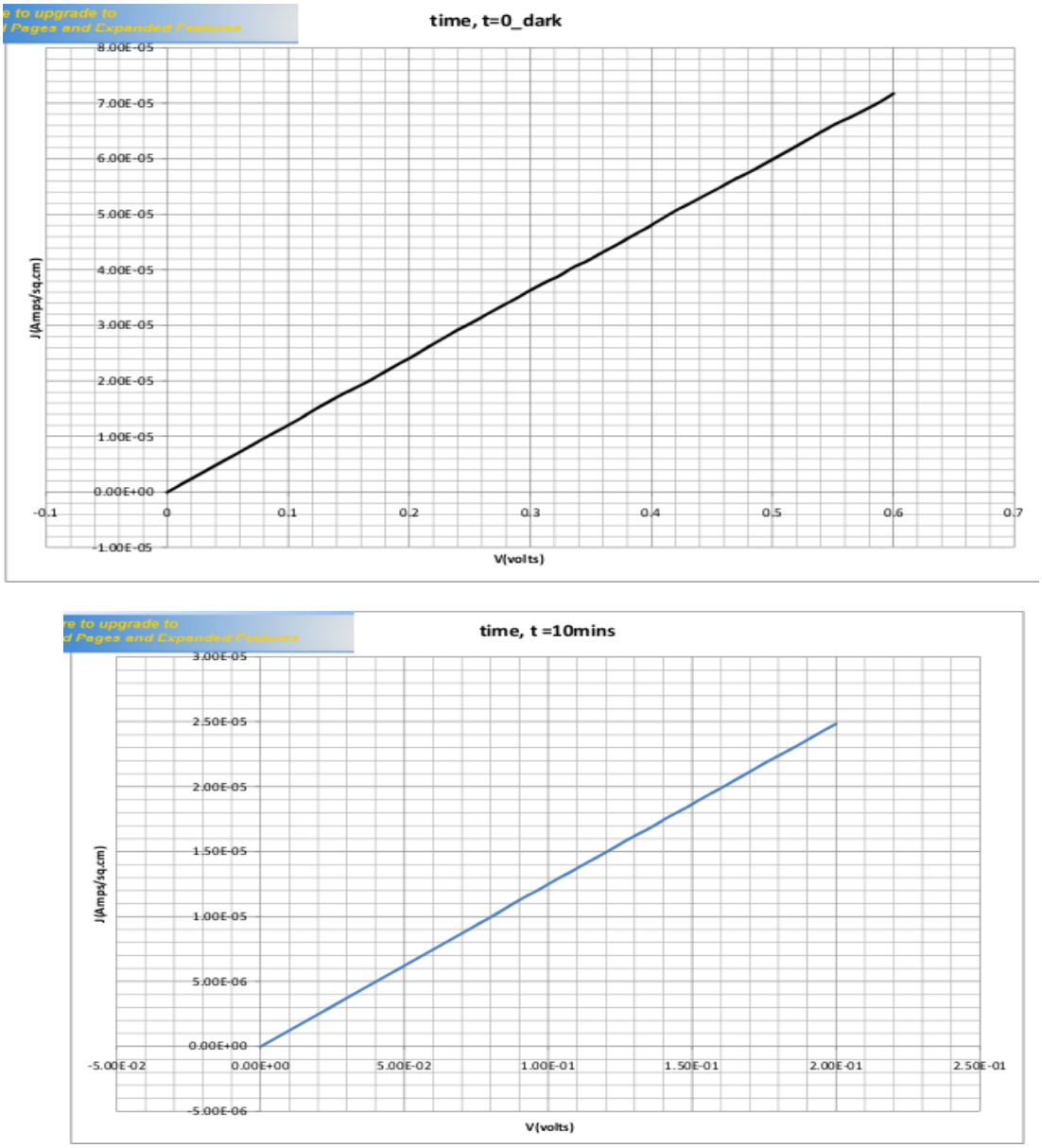

Fig 3.13: Dark characteristics observed for a ITO/PEDOT;PSS/P3HT;PCBM/Al device with active layer spincoated from a 10mg/ml solution. a) initially b) after 10 minutes.

Figure 3.14 shows results for the solar cell under illumination for the three times. the short circuit current density J_{sc} and the open circuit voltage V_{oc} values of $25\mu A/cm^2$,$14\mu A/cm^2$, $10\mu A/cm^2$ and 0.2V, 0.12V, 0.6V were respectively obtained for all three times. A comparison of these three show values decreasing with time and thus the device can be said to be unstable in this time.

Figures 3.15a shows the J_{sc} values as a function of time while Figure 3.15b shows J_{sc} as a fraction of initial J_{sc} values also as a function of time. These further buttress the degradation of the device with time.

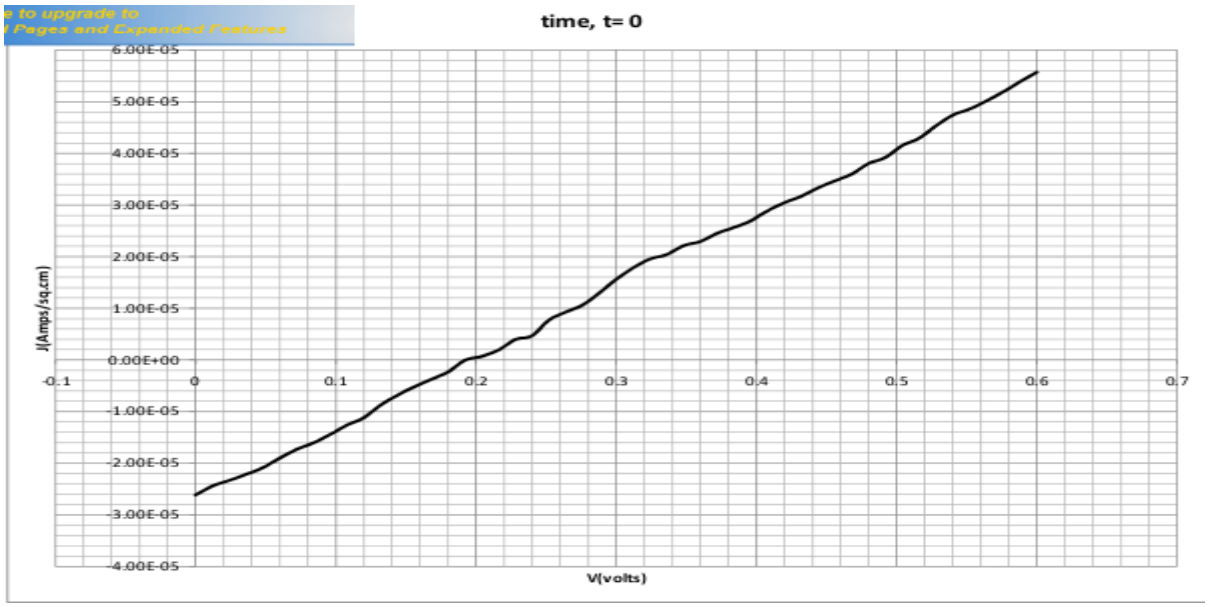

(a)

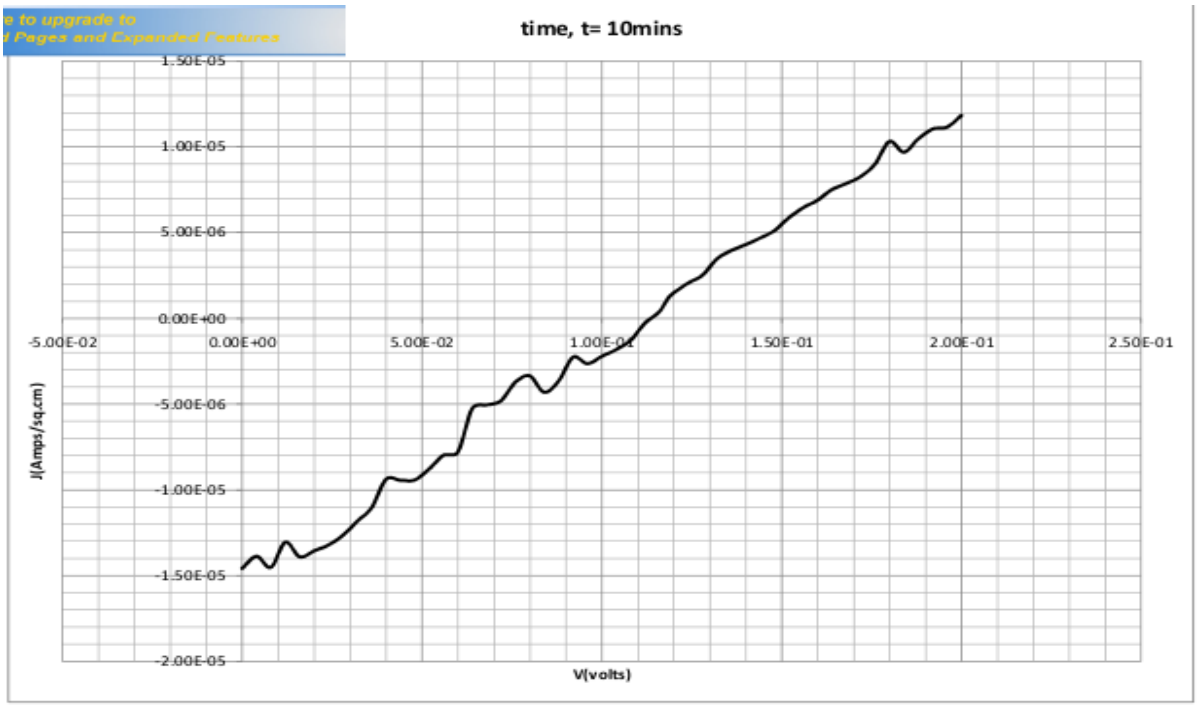

(b)

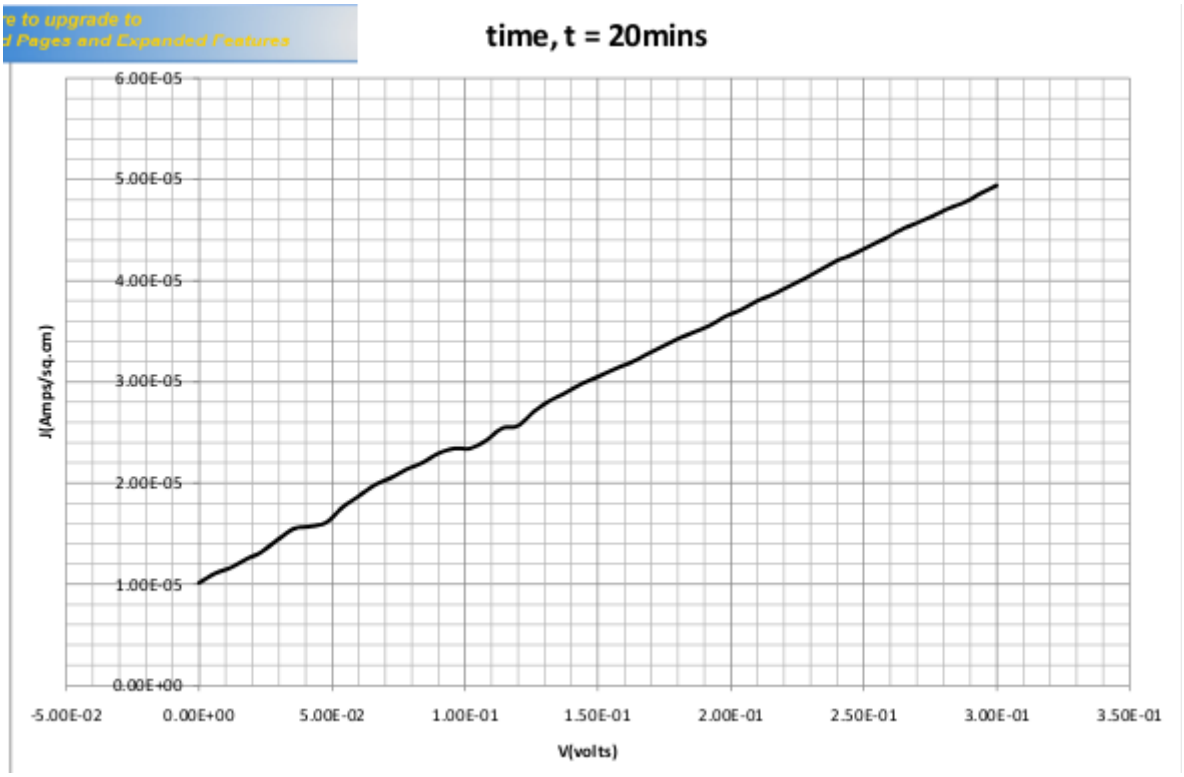

(c)

Fig 3.14: Light characteristics observed for a ITO/PEDOT;PSS/P3HT;PCBM/Al device with active layer spincoated from a 10mg/ml solution. a) initially b) after 10 minutes c) after 20 minutes.

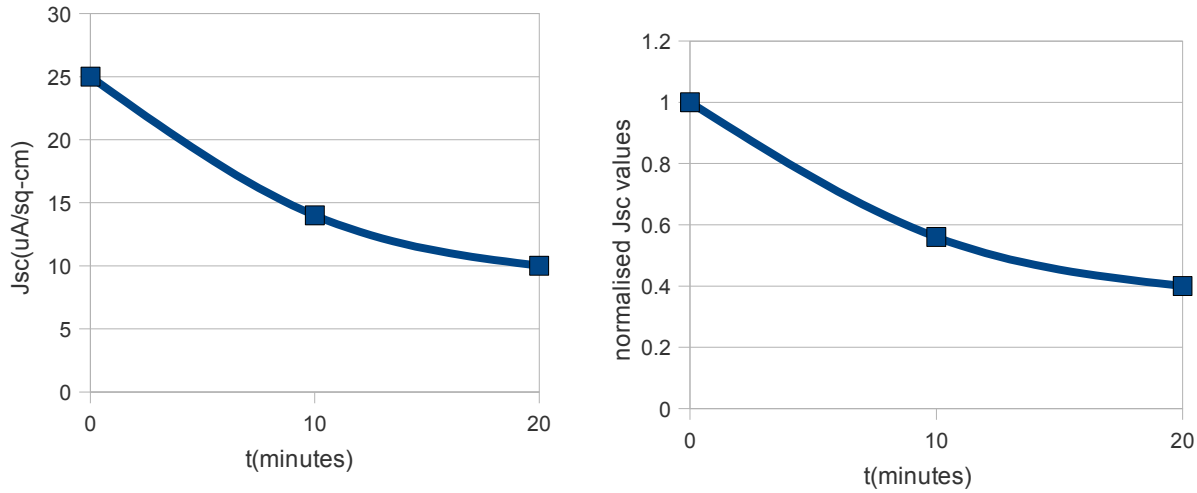

Fig 3.15: Degradation features of the device. a) Real values as a function of time. b) Normalised values as a function of time.

ITO/P3HT:PCBM/Al

This device was also analysed for the purpose of comparison with the one above. The difference between these is the absence of the PEDOT:PSS layer which enhances the transport of holes to the anode but however leads to an increased degree of degradation being hygroscopic. It's J-V characteristics were also taken and the degradation pattern observed. Fig 3.16 shows the J-V characteristic curve observed for times, zero, and ten minutes respectively.

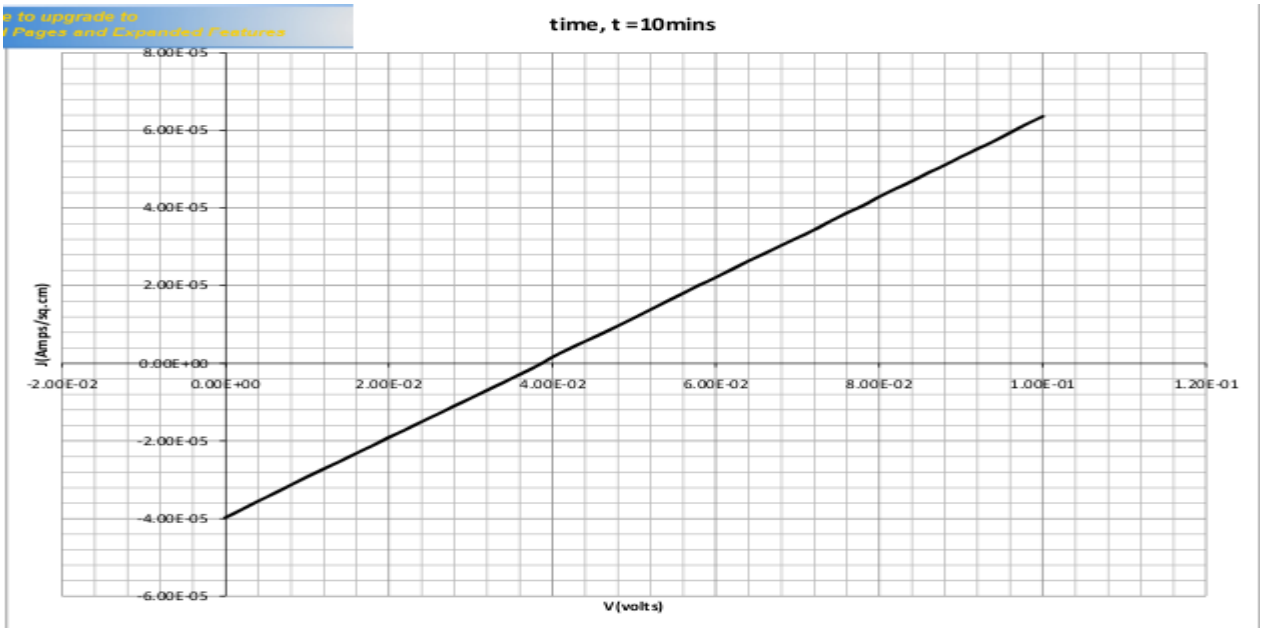

Fig 3.16: J-V characteristic curves for a ITO/P3HT:PCBM/Al device. a) at start of illumination b) ten minutes after illumination.

The figures show the J-V curves at time t=0 and t=10minutes with J_{sc} and V_{oc} values of 50uA/sq.cm, 0.07V and 40uA/sq.cm, 0.38V respectively. The fact that the J_{sc} value decreases is an indication that the device also degrades in time. At time t = 10minutes, the J_s value is about 57% of the initial value. Comparing this to the ITO/PEDOT;PSS/P3HT;PCBM/Al where this quantity is 56%, it is observed that these values are very close.

Specimen 2

ITO/PEDOT:PSS/P3HT:PCBM/Al

This is the second specimen analysed in this work. The fabrication was similar to the above, except for the active layer spin coating conditions which are state above and the active device area which was about 0.5*0.5 sq.cm. For the J-V characteristics varying sweep voltages were used and results observed over time are shown below in figures 3.17. As expected, the J_{sc} and V_{oc} values also decrease with time.

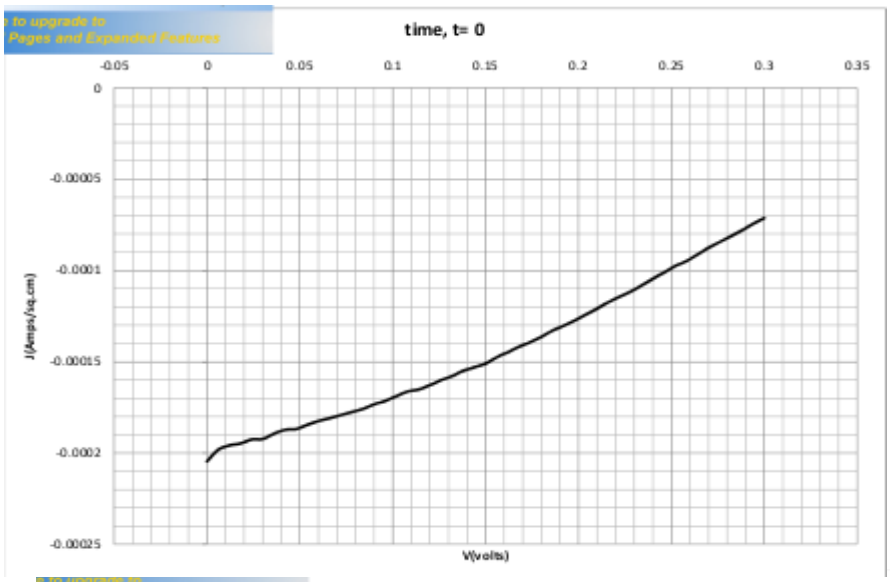

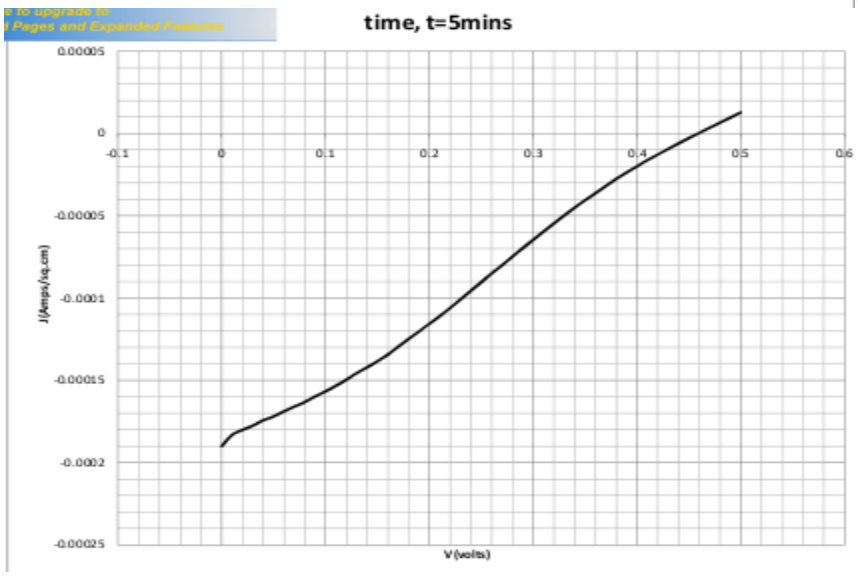

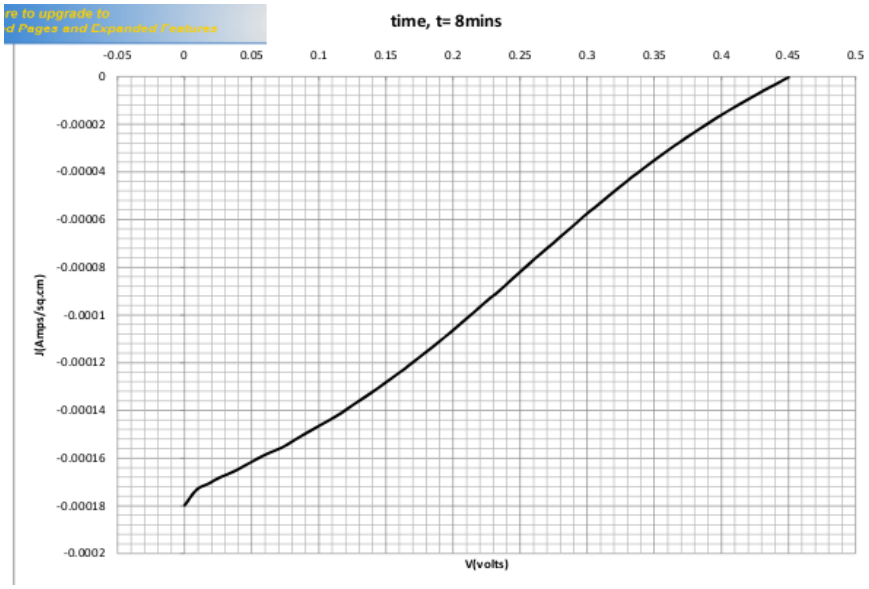
time, t= 8mins
-0.05
0
0.05
0.1
0.15
0.2
0.25
0.3
0.35
0.4
0.45
0.5
0
-0.00002
-0.00004
-0.00006
-0.00008
-0.0001
-0.00012
-0.00014
-0.00016
-0.00018
-0.0002
J(Amps/sq.cm)
V(volts)

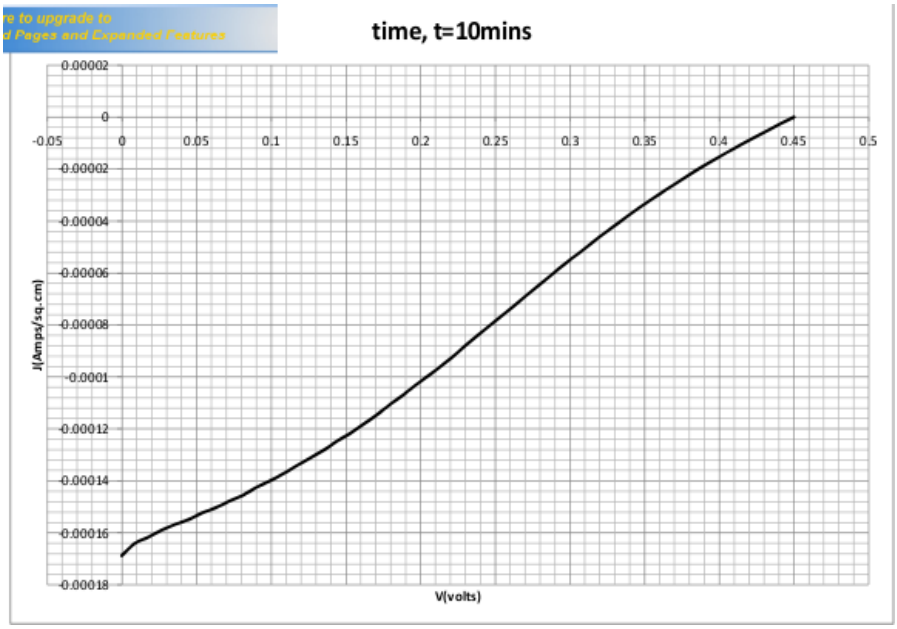
time, t=10mins
0.00002
0
-0.05
0
0.05
0.1
0.15
0.2
0.25
0.3
0.35
0.4
0.45
0.5
-0.00002
-0.00004
-0.00006
-0.00008
-0.0001
-0.00012
-0.00014
-0.00016
-0.00018
J(Amps/sq.cm)
V(volts)

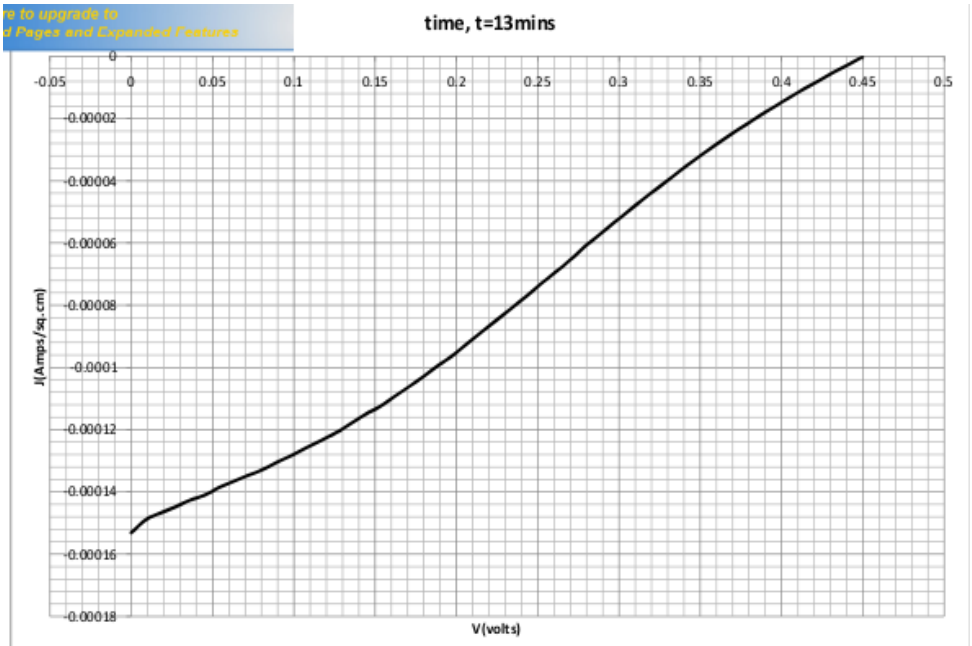
time, t=13mins
J(Amps/sq.cm)
V(volts)

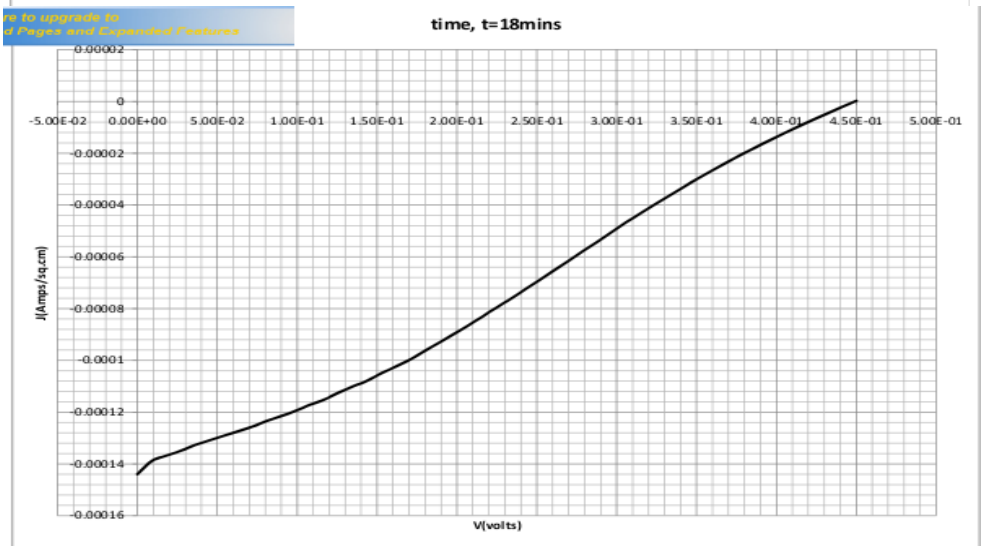
time, t=18mins
J(Amps/sq.cm)
V(volts)

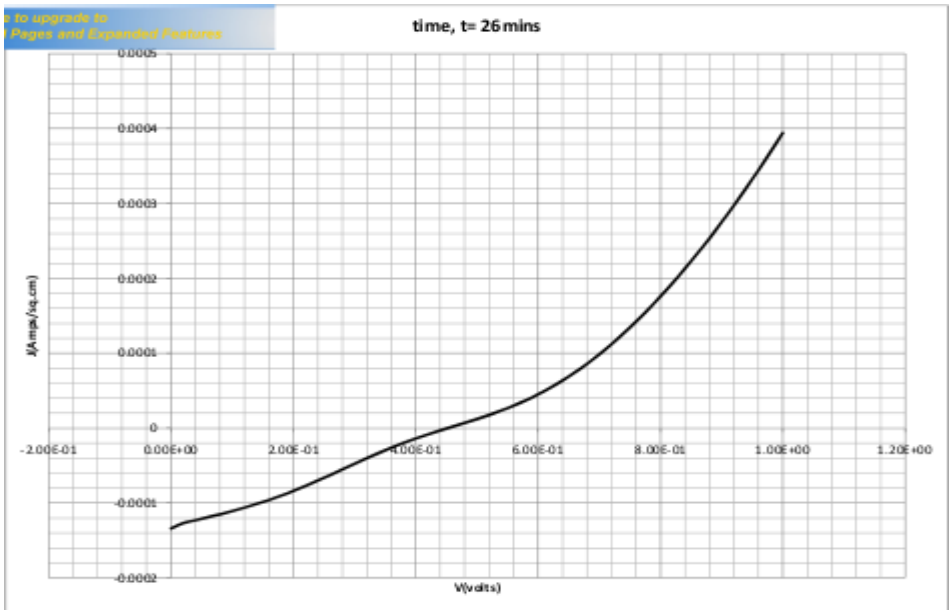
time, t= 26 mins
J(Amps/sq.cm)
V(volts)

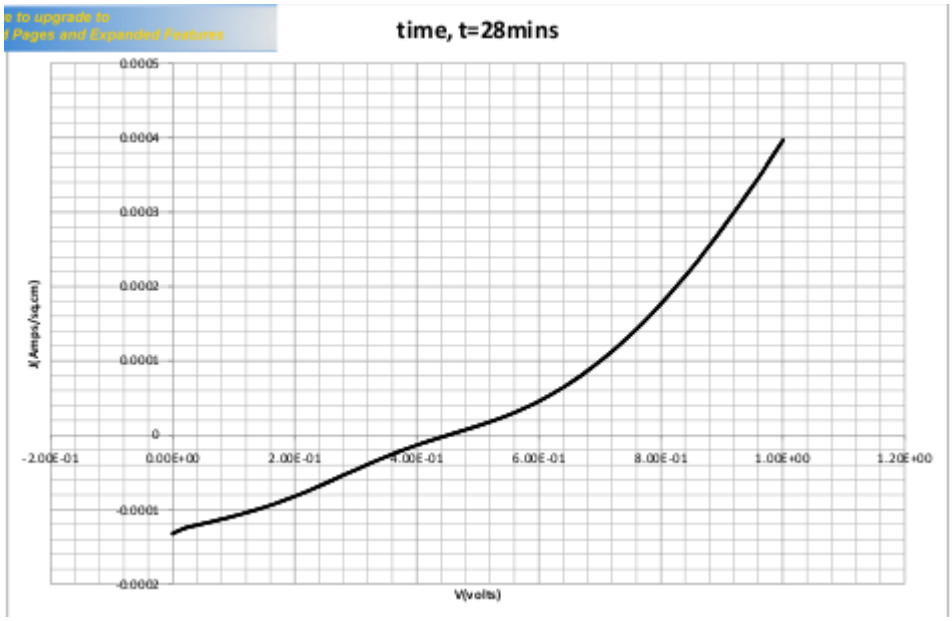
time, t=28mins
J(Amps/sq.cm)
V(volts)
0.0005
0.0004
0.0003
0.0002
0.0001
0
-0.0001
-0.0002
-2.00E-01
0.00E+00
2.00E-01
4.00E-01
6.00E-01
8.00E-01
1.00E+00
1.20E+00

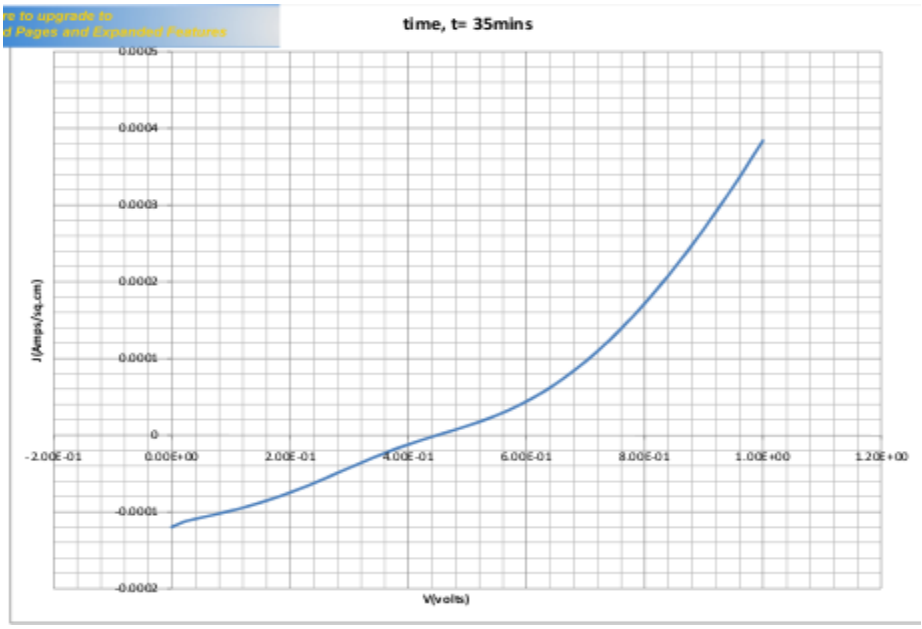
time, t= 35mins
J(Amps/sq.cm)
V(volts)
0.0005
0.0004
0.0003
0.0002
0.0001
0
-0.0001
-0.0002
-2.00E-01
0.00E+00
2.00E-01
4.00E-01
6.00E-01
8.00E-01
1.00E+00
1.20E+00

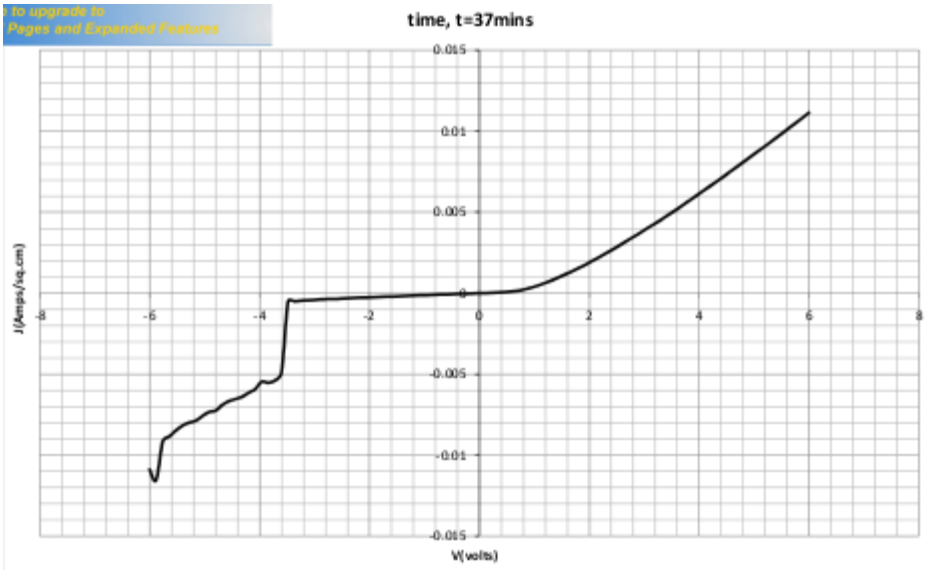
time, t=37mins
J(Amps/sq.cm)
V(volts)
0.015
0.01
0.005
0
-0.005
-0.01
-0.015
-8
-6
-4
-2
0
2
4
6
8

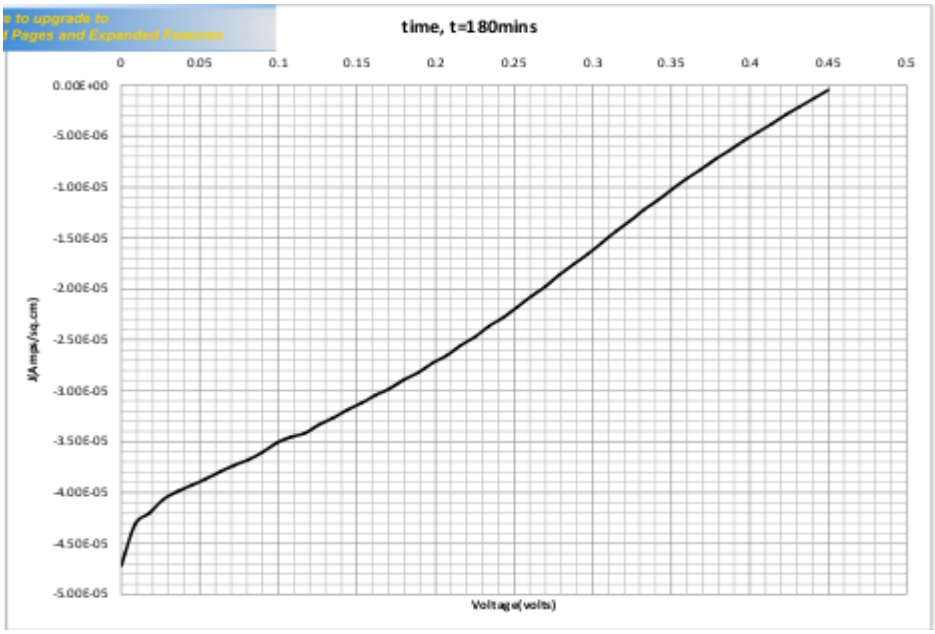

Fig 3.17: J-V characteristics of a Specimen 2 made from a 20mg/ml solution of P3HT:PCBM blend.

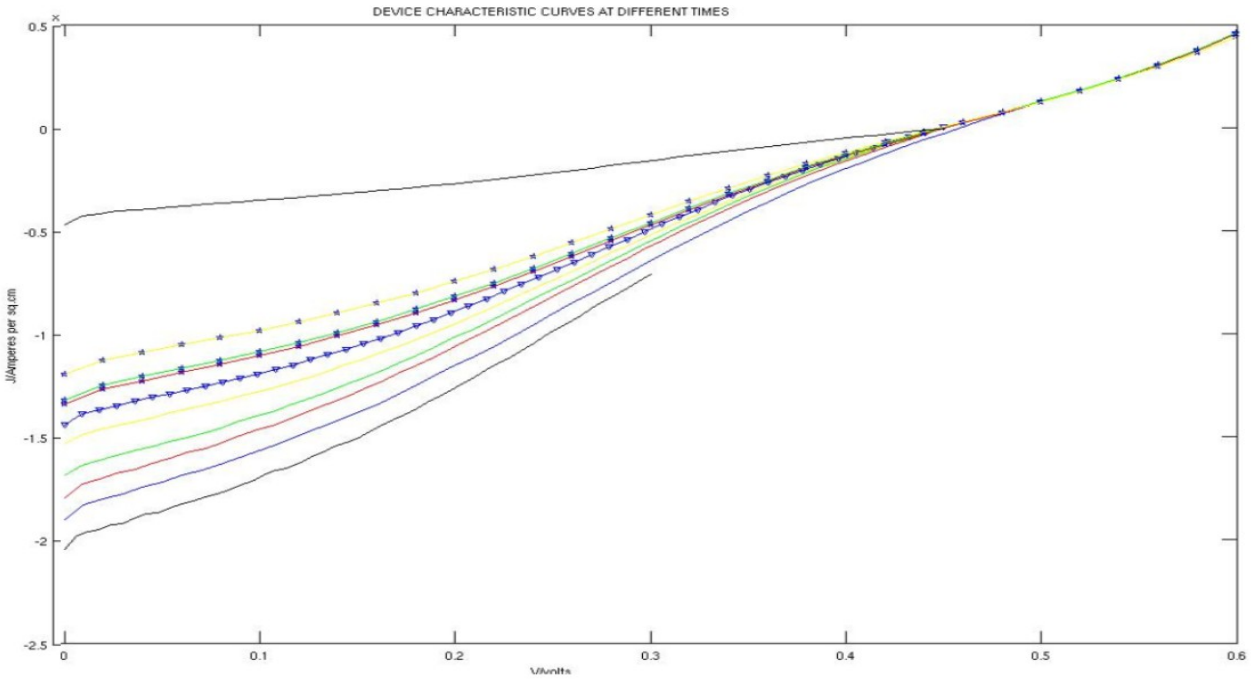

Fig 3.18:J-V characteristics for all times showing higher time observations above lower ones.

The degradation curve is again derived from the above by plotting the current density and normalised current densities against time and is shown below in Figure 3.19a and b respectively.

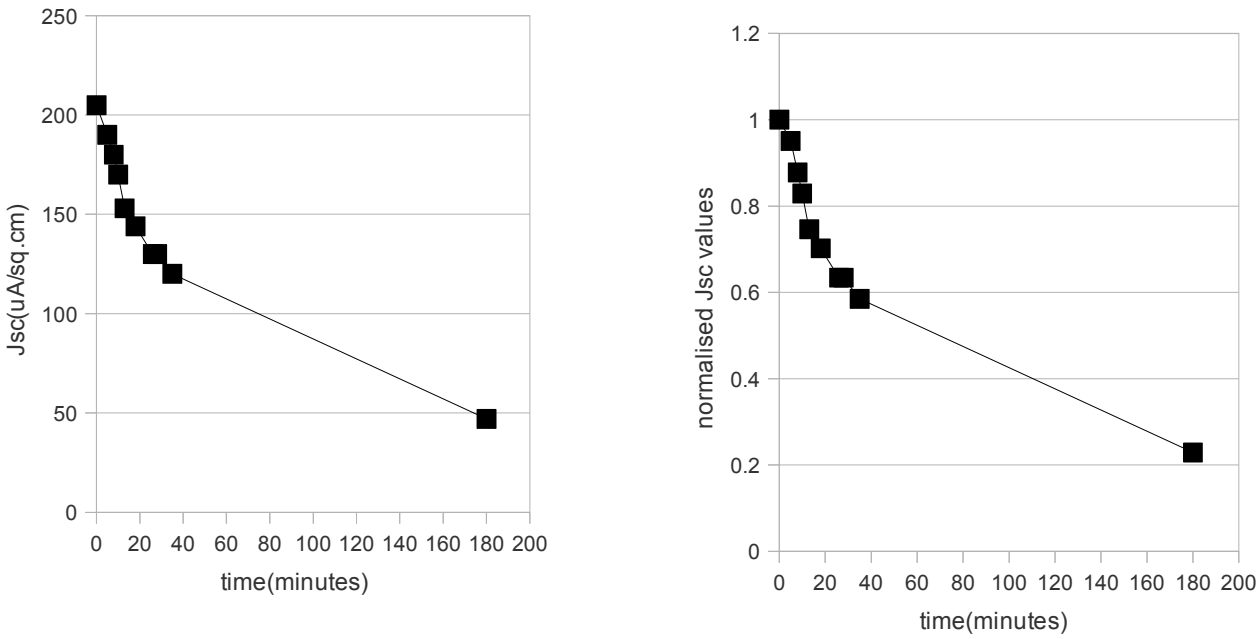

Fig 3.19: Degradation features of the device. a) Real values as a function of time. b) Normalised values as a function of time.

The highest J_{sc} value observed during initial illumination is 205µA/sq.cm and this decreases progressively. This is much larger when compared with Specimen 1, where it was only 25µA/sq.cm, And after 20 minutes, the J_{sc} value for specimen 2 is still about 70% the initial value, whereas that of specimen 1, as at 20minutes was already 40%. Hence it can be reasonably concluded that specimen 2 is more stable than specimen 1.

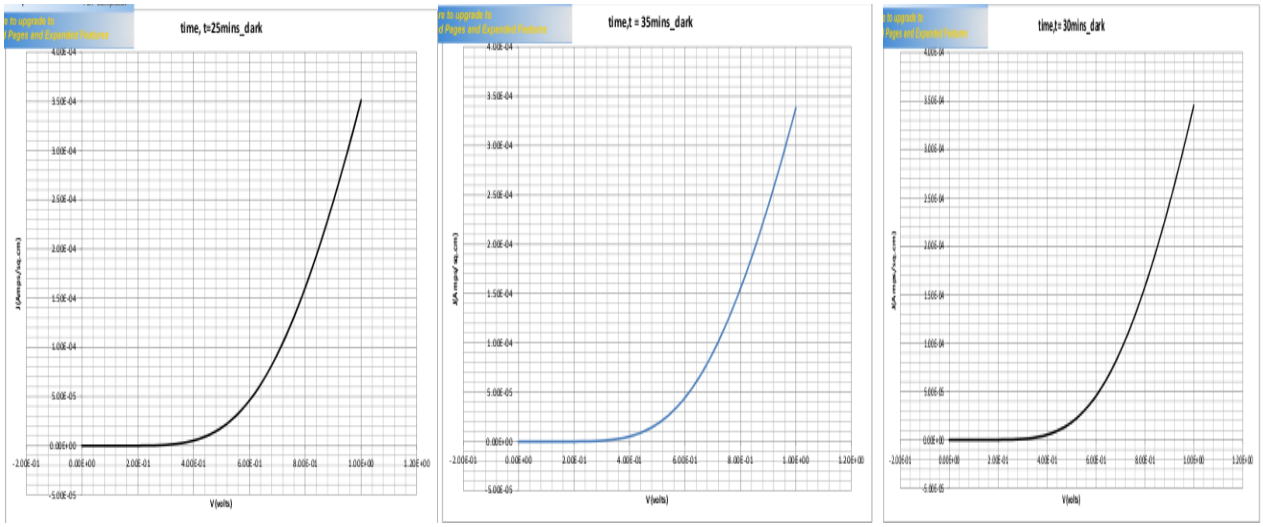

Fig 3.20: J-V characteristics obtained in the dark at times a) t=25mins b) t=30mins c) t=35mins after illumination.

3.6.2 SEMI-DEVICES

ITO/PEDOT:PSS/P3HT:PCBM- A look at the effect of annealing.

On deposition of the active layer on the PEDOT:PSS, the roughness, sheet resistance and transmittance were observed. Two samples, one baked under conditions stated above and the other, unbaked were investigated.

The transmissivity results for both are shown in the figure below. The figure shows that the unbaked specimen is generally about 5% more than the baked for wavelengths greater than 400nm. This implies that the absorption of the baked specimen will be greater in the baked for the same reflective power in both.

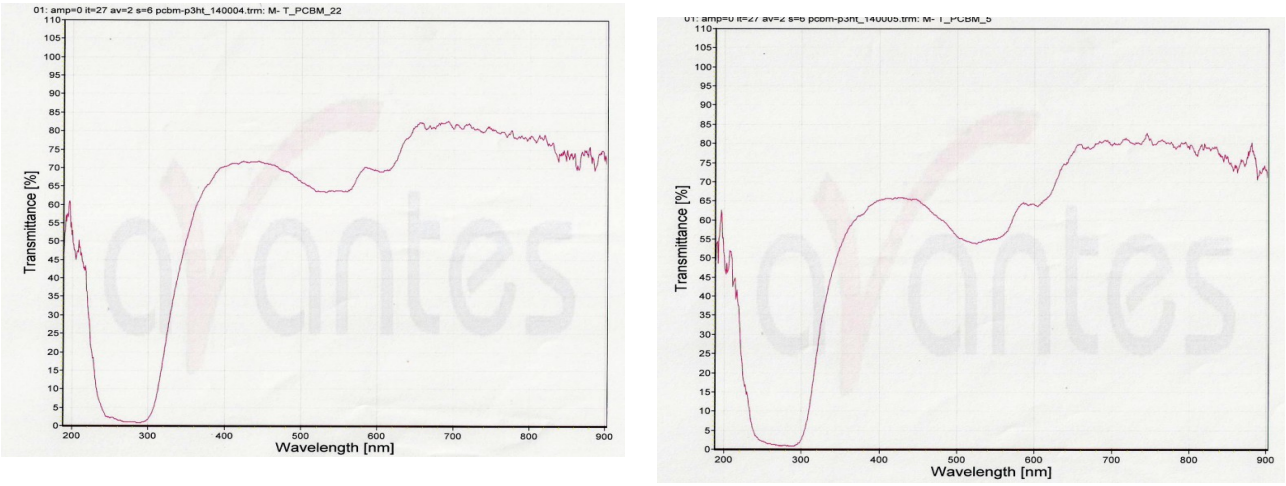

Fig 3.21: Transmittance of P3HT:PCBM thin films deposited on glass substrate a) specimen baked after spin coating. b) specimen unbaked after spin coating.

The roughness profile of them both was also taken and fig 3.20 below shows this. The roughness averages observed are quite similar with 4.59nm and 4.66nm for the unbaked and baked respectively i.e. just a difference of <1°A. This implies that although one expects a difference as a result of grain growth and formation of defects, the difference observed is quite small hence for studies which depend strictly on the morphology of the active layer surface such as adhesion measurements, it is immaterial whether the active layer is baked or not, after spincoating.

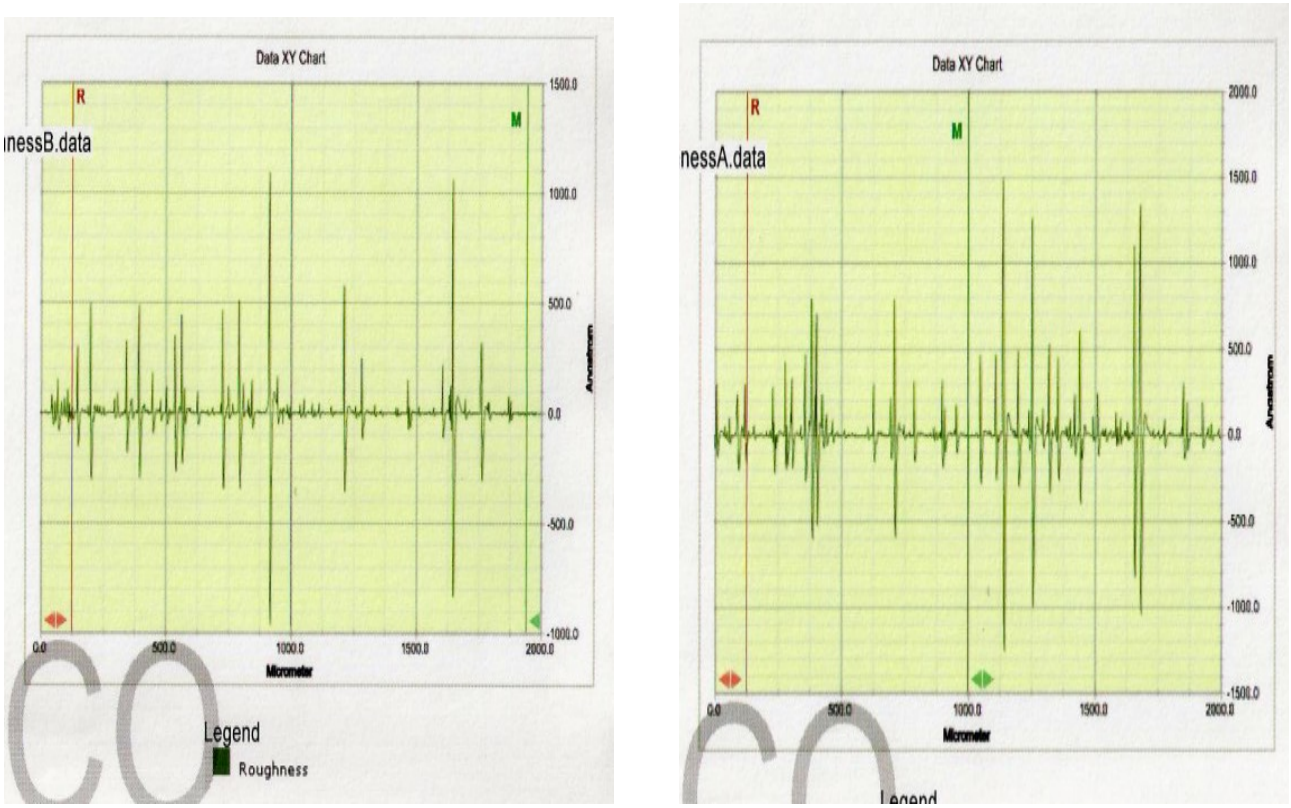

Fig 3.22: Roughness profile for the unbaked and baked samples, respectively.

PEDOT:PSS ON GLASS

The properies of the pedot:pss used were also investigated by spincoating it on plane glass under spincoating conditions stated above. The transmittance curve of the specimen(fig) showed a transmittance of over 80nm in the range of 350nm<λ<750nm relative to air although it appeared opaque to wavelenghts less than 300nm. This is very similar to that obtained for plane glass which was generally ~5% more for wavelenghts greater than 350nm. This shows that the pedot:pss was not likely to hinder the required transmittance of light to the active layer.

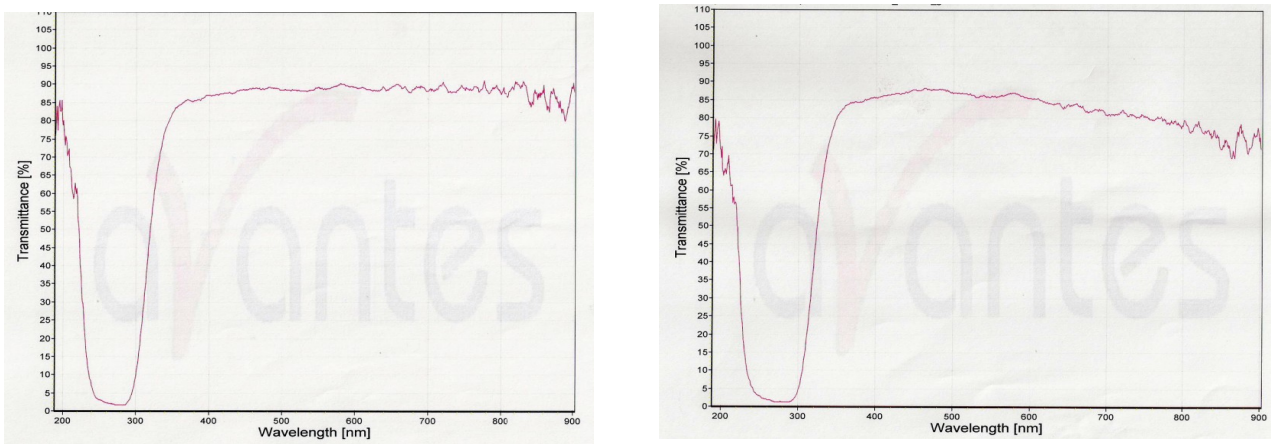

Fig 3.23: Transmittance for a)plane glass and b)pedot:pss on glass.

The roughness profile, scanning electron micrograph and energy dispersive xray spectroscopic data are also shown below. The roughness average for the pedot:pss is observed to be 3.2nm while its thickness was observed to be ~100nm from fig 3.24d and 3.24c respectively. The EDXRF results showed the presence of K, Ca, N, O_2,Na, Mg, S, Al and Si. Although only C, O_2 and S were expected, the resolution used for the probe may have led to elemental components of the glass substrates being observed too.

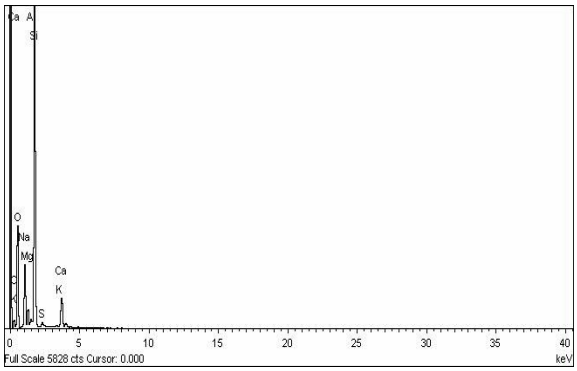

(a)

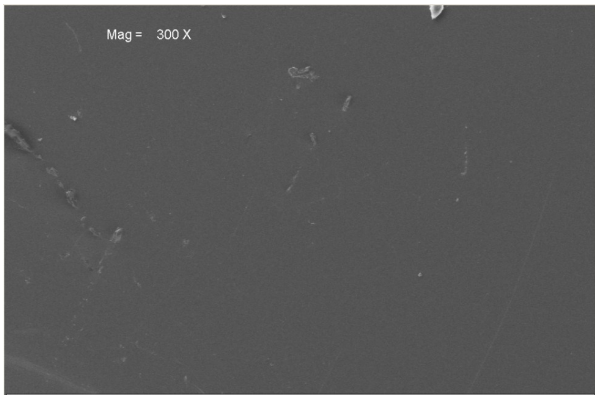

(b)

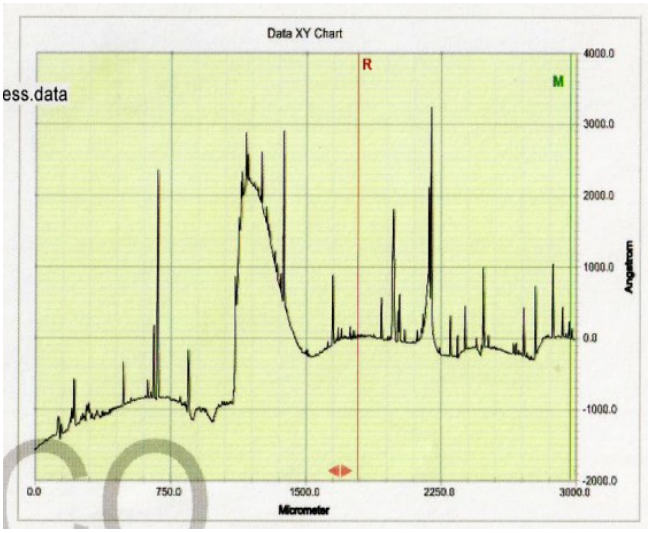

(c)

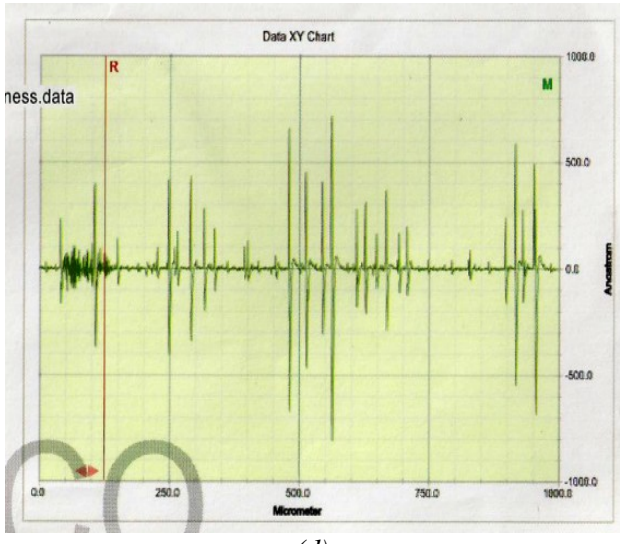

(d)

Fig 3.24: a) EDXRF results b) SEM image c) thickness profile d) roughness profile, for the PEDOT:PSS coated glass

P3HT:PCBM ON GLASS

Analysis of specimens of the active layer spincoated on plain glass showed very interesting results. The transmittance results in fig 3.23 show that the specimen produced from the 20mg/ml(specimen 2) solution was much more opaque to light than the 10mg/ml(specimen 1)one. For wavelengths between 230nm and 630nm, the former had a zero percent transmittance while the later had about between 25 and 55% transmittance in this region. For wavelengths greater than 630nm, specimen 2 was about 20% more transmissive than specimen 1. Wavelengths of visible light is usually more concentrated in the 200nm to 700nm region and the lesser the transmittance of the active layer in this region, the more the absorptance and consequently the better the material for use as an active layer hence for every other factor being held constant, the specimen 2 will yield a better end device.

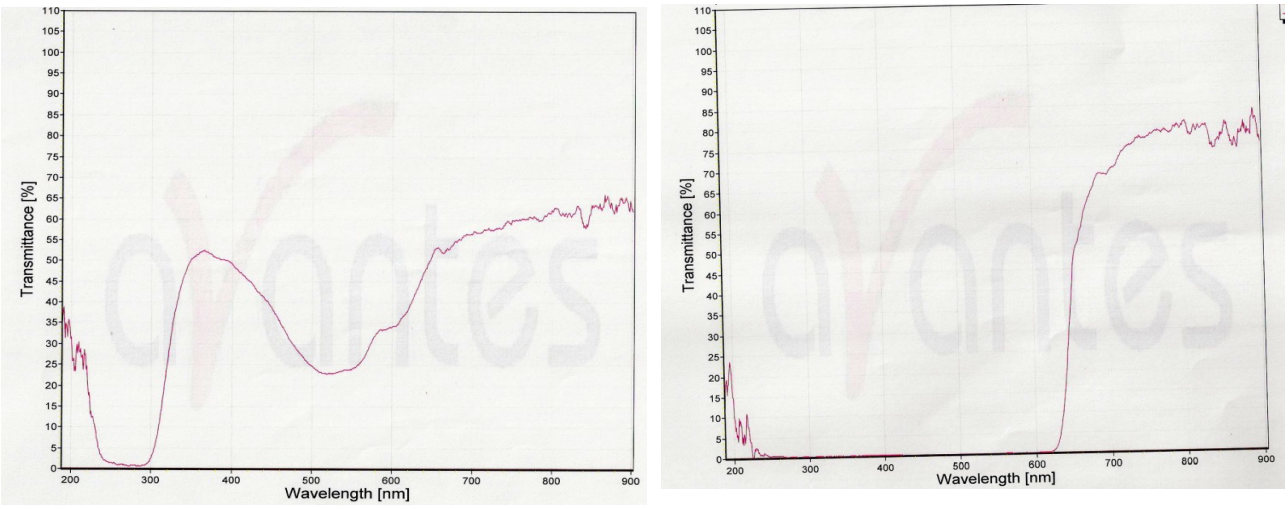

Fig 3.25: Graph of transmittance against wavelength for PCBM:P3HT specimen based on a) 10mg/ml solution b)20mg/ml solution.

The roughnesses of both specimen observed from the surface profiler are shown in fig 3.26a and b. An order of difference was observed in the roughness average of the two samples. This is due to the fact that the solution had to be spincoated and baked for four different times in order to get the desired thickness in specimen 1.

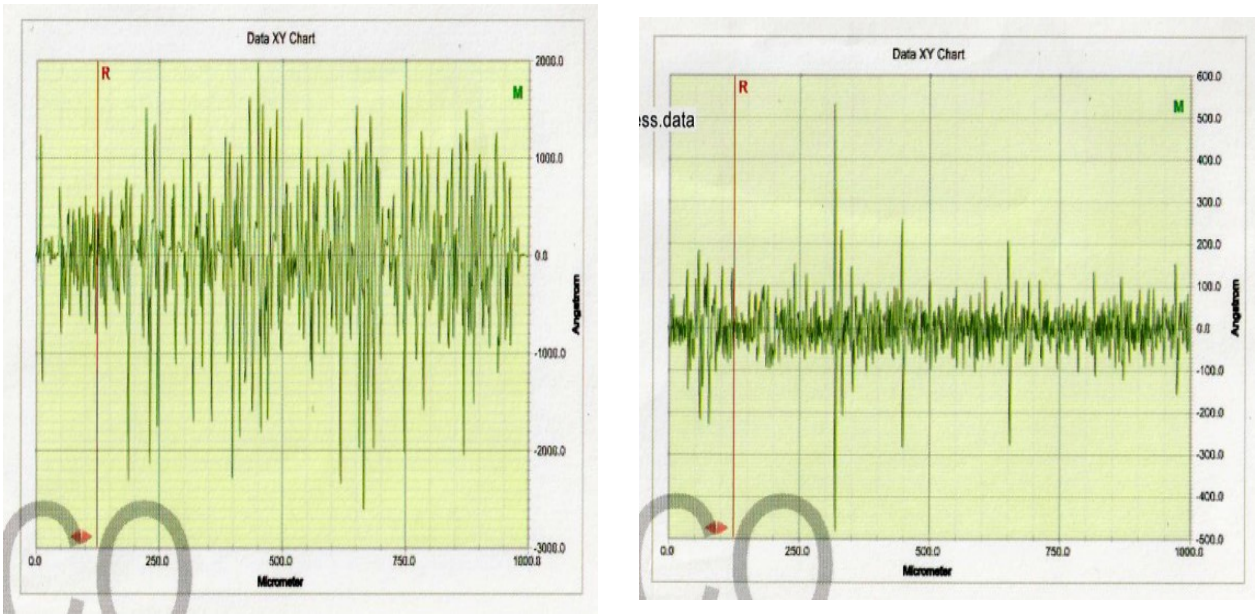

Fig 3.26: Roughness profile for a) 10mg/ml solution deposited on glass(roughness average=43.31nm) b) 20mg/ml solution deposited on glass(roughness average=3.59nm).

The scanning electron micrograph for both specimens are also shown below. The darkness of specimen 2 relative to specimen 1 further shows the opacity of specimen 2 relative to 1.

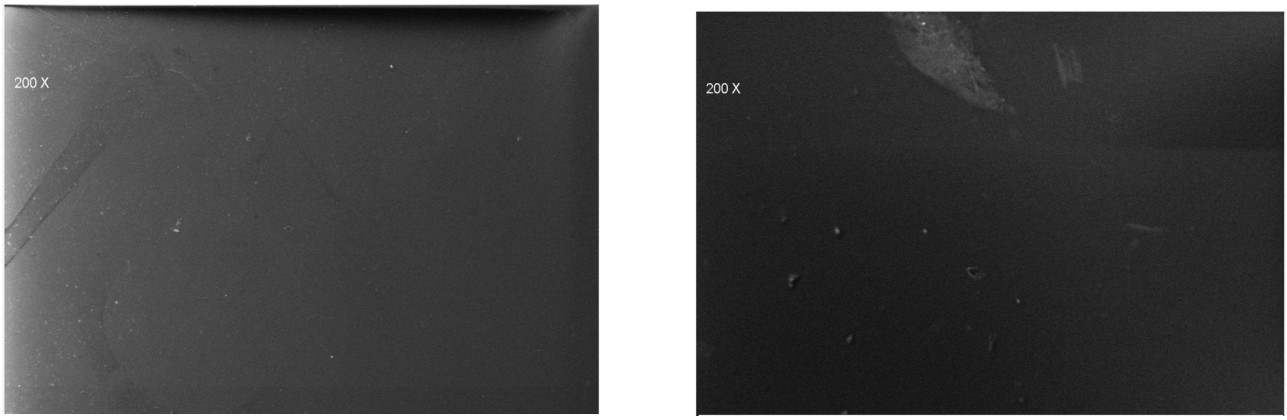

Fig 3.27: SEM of P3HT:PCBM spincoated on plain glass at a)10mg/ml solution b)20mg/ml solution

3.7 FURTHER DISCUSSIONS

The degradation trends observed generally in organic solar cells is due to several sources which cause an evolution in the bulk heterojunction microstructure . Fractal dendritic structures form with time and these reduce the distribution of the pcbm structure, then the degree of charge hopping in the bulkheterojunction layer and eventually the effective charge transport. Fig 3.28 shows a typical bulkheterojunction layer observed under a scanning electron microscope with time. The dendritic structures formed can be clearly seen.

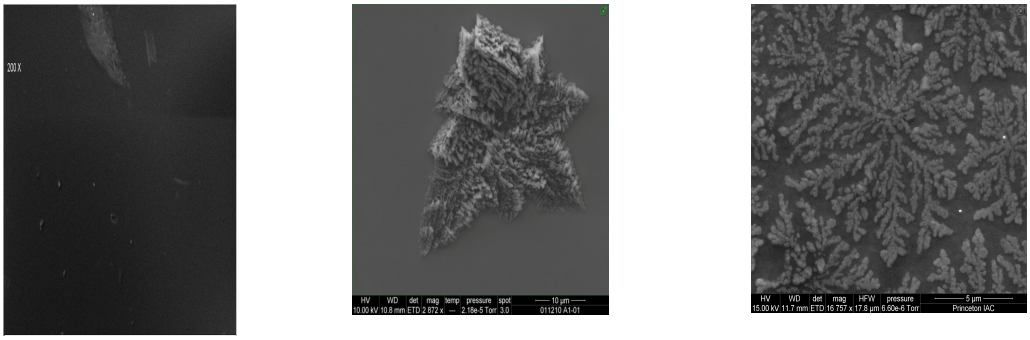

Fig 3.28: A typical bulkheterojunction layer observed under a scanning electron microscope with time

As also observed from the morphology tests, the degree of roughness can also tell a lot about the

device performance. If the thin film layers are too rough, the degree of adhesion between layers at interfaces may be too small and this will affect the charge transport between layers to the electrodes and consequently the efficiency and lifetime. Hence thin film layers should be deposited under conditions which minimize roughnesses.

SUMMARY, CONCLUSIONS AND RECOMMENDATIONS.

Typical OPVs based on P3HT:PCBM polymers have been fabricated and effectively characterised to observe and compare the degradation trends. The following were the major procedure. The study was carried out in three different stages.

- Device fabrication
- Optical and morphological characterisation
- Electrical characterisation.

For the device fabrication, OPVS prepared consisted of the electrodes, an active layer (P3HT:PCBM) with an additional PEDOT:PSS layer serving as a hole conducting layer and it was concluded that the various conditions at which each thin layer is deposited is important for the device performance.

The optical characterisation of each thin film layers deposited on glass gave results which showed their various contributions to the absorbance of the main device and also showed the active layer of specimen 2 to be a better absorber compared to specimen 1.

The surface morphology of the various layers were also observed both relative to plain glass and to the preceding layer. The degree of roughnesses were a function of the deposition and annealing conditions and these roughnesses could affect the charge transport through and the interface between layers.

For the electrical characterisation, the J-V characteristics curves showed good results. Especially for specimen 2 which exhibited diodic characteristics as expected when observed in the dark.
For specimen 1 i.e ITO/PEDOT:PSS/P3HT:PCBM/Al and ITO/P3HT:PCBM/Al samples, both were observed to exhibit similar degradation trends however specimen 2 was observed to be much more stable than specimen 1 as it's degradation was much slower hence we were able to conclude that a device fabricated under conditions of specimen 2 will exhibit a better performance than that of specimen 1.

Table 4.1 gives a summary of the observations on both specimen.

Summary

	Specimen 2	Specimen 1
Active layer concentration	20mg/ml	10mg/ml
Active device area	0.25sq.cm	1sq.cm
Spincoating times	1	4
Roughness average value	3.59nm	43.31nm
Initial J_{sc} value	205µ A/sq.cm	25µ A/sq.cm
%age of J_{sc} left after 20 minute exposure	56.00%	40.00%
Behaviour	Diodic	Ohmic
Summary	Better	Good

Table 4.1: Summary of conditions and observations for both specimen.

Degradation of the J-V characteristics was due to various sources which eventually lead to the evolution of dendritic structures, a reduction in the distribution of PCBM structure, a decrease in the degree of charge hopping in the bulkheterojunction layer and consequently a reduction in the effective charge transport.

This project has looked at the characteristics of different layers of the solar cell, the properties of each component deposited on glass and concluded that most of the features observed generally agree with the earlier on expected results.

The electrical characteristics of the devices studied also behave as expected, ie when considering the characteristics and the degradation of the current densities with time.

However, a lot of work still needs to be done. Further modification of fabrication processes, such as annealing times, spin coating conditions, thin film layer sizes, device geometry, activelayer blending time, and even the source of products could be modified to still verify if results could be similar and if better results could be obtained.

The greatest breakthrough in P3HT:PCBM cells will depend on the adequate use of the P3HT:PCBM phase diagrams to predict an optimum composition and temperature for its active layer preparation. A work devoted to that might bring about an optimum methodology which will go a long way in topping the current efficiency peak and improving the stability of the device.

The morphological tests carried out is not such an excellent way of depicting roughnesses of the general specimen area as the analysed portion is just a minute portion of the entire surface. A more accurate test will be to take the 3D surface profile or taking the roughness averages for several separate regions and then taking the average of the results obtained.

For this work, we have assumed zero reflectance for absorption calculations which is not practically correct. Future works should take cognisance of the reflectance so that the exact absorptance values are obtained.

Dichlorobenzene could be used instead of chlorobenzene used here as it has been shown to produce superior devices when used and then degradation trends could be observed over longer periods of times.

REFERENCES

1. Hong Ma, Hin-Lap Yip,Fei Huang, Alex K.-Y Jen* ; Interface Engineering for Organic Electronics; Advanced functional materials journal.
2. G. Li, V. Shrotiya, J.S. Huang, Y. Yao, T. Moriarity, K. Emery, Y. Yang. Nature materials 2005, 4, 864.
3. W.L. Ma, C.Y. Yang et al, Advancedfunctional materials 2005, 15,1617
4. S. Chaudhary, H.W Lu, A.M. Muller, C.J. Bardeen, M. Ozkhan, Nanoletters 2007, 7, 1973
5. J. Y. Kim, S.H. Kim, H.H. Lee, K. Lee, W.L Ma, X. Gong, A.J. Heeger, Advanced functional materials, 2006, 18,572.
6. Martin Drees; Polymer/Fullerene photovoltaic devices- nanoscale control of interface by thermally controlled interdiffusion. 2003.
7. L. Chen, D. Godovsky, O. Inganas, J.C. Hummelen, R.A.J. Janssen, M. Svensson, M.R. Andersson. Polymer photovoltaic devices from stratified multilayers of donor-acceptor blends; Advanced materials 12(18), 1367-(2000)
8. C.J. Brabec, A. Cravino, D. Meissner, N.S. Saricifti, M-T Rispens, L. sanchez, J.c. Hummelen, T. Fromherz, “The influence of materials work function on the open circuit voltage of plastic solar cells”, thin solid films403-404, 368-372(2002)
9. D. Vacar, E.S. Maniloff, D.W. Mcbranch, A.J. Heeger, “Charge transfer range for photoexcitons in conjugated polymer/fullerene bilayers and blends” Phys-Rev B, 56(8), 4573-4571(1997)
10. J.J.M. Halls, K. Pichler, R.H. Friend, S.C. Moratti, A.B. Holmes, “Exciton diffusion and dissociationin a poly(p-phenylenevinylene)/C_{60} heterojunction photovoltaic cell”, Appl. Phys. Lett. 68(22), 3120-3122(1996).
11. Arun Tej Mallajosyulla, Naveen Srivasta, S. Sundar Kumar Iyer, Baquer Mazhari; “Characterisation of matrix and isolated organic cells: solar energy materials and solar cells, 94(2010), 1319-1323
12. Jing. Shun Huang, Chieh-Yu Hsiao, Shu-Jia Syu, Jiun-Jie Chao, Ching-Fuh Lin; “Well alligned single crystalline nanowire hybrid solar cells on glass”
13. Heejo Kim, Won-Wook So, Sang-Jin Moon;“Effect of Thermal annealing on Performance of P3HT:PCBM polymer voltaic cells. Journal of the Korean Physical Society(2006), Vol. 48, No. 3, pp 441-445
14. Wole Soboyejo, 'Frontiers in Science and Technology for African Development'.
15. S. Dantip, Y. Hoshi, Y. Kasahara, Y. Onai, T. Osotchan, Y. Sawada; Study of low power

deposition of ITO for top emission OLED with facing target and Rf sputtering systems", Journal of Physics, conference series 100(2008)

16. M.G. Zebaze Kana, E.Centurioni,D. Iencinelle, C. Summonte: "Influence of the sputtering system's vacuum level on the properties of ITO films"
17. l
18. Ge Weihao," An overview of P3HT:PCBM, the most efficient organic solar cell material so far".
19. Sigma Aldrich product information. Catalog number 698997; Technical bulletin AL-250.
20. Chun-Hao Huang, Chia-Hao Huang, Thien-Phap Nguyen, Chain-Shu Hsu, "Self -assembly mono layerof Anatase TiO2 for solution process of ITO glass substrate for polymer PV cells"
21. T. Tong, B. Babatope, S. Admassie, J. Meng, O. Akogwu, W. Akande, W.O. Soboyejo, "Adhesion in organic electronic structures"
22. Eleanor Ramsden and Phillippi Uttley, "Organic PV solar cells", www.livescience.com
23. Kenji Kawano, Roberto Pacios, Dmitrry Poplavskyy, Jenny Nelson, Donal D. C. Bradley, James R. Durrant, "Degradation of Organic Solar cells due to air exposure".
24. Rivers N.P. , "Leading edge research in solar energy"(2007)
25. Holger Spangggnard, Frederik C. Krebo"A brief history of the development of organic and polymeric voltaics".
26. Lhadi Merhari "Hybrid nanocomposites for nanotechnology-electronic, optical, magnetic and biomedical applications".
27. T. Chi, T. Ballinger, R. Olds, M. Zecchino, "Surface texture Analyss using Dektak stylus profilers"
28. Waldo J.E. Beek, Martjin M. Wienk, Reno A.J. Jannsen. "Efficient Hybrid solar cells from ZnO nanoparticles and a conjugated polymer"
29. C. W. Tang, Applied Physics letters. 48(1986) 183.
30. M. Hiramoto, H. Fukusumi, M. Yokoyama, Applied Physics letters, 58(1991) 1062
31. N.S. Sacrifitci, L. Smilowitz, A.J. Heger. F. Wudl. AppliedPhysics letters, 62(1993) 585.
32. L. Schmidt-Mende, A. Fectenkotter, K. Mullen, E. Moons, R.H. Friend, J.D. MacKenzie, Science 293 (2001) 1119.
33. G. Yu, K. Pakbaz, A.J. Heeger, Appl. Phys. Lett. 64 (1994) 3422.
34. G. Yu, J. Gao, J.C. Hummelen, F. Wudl, A.J. Heeger, Science 270 (1995) 1789.
35. P. Schilinsky, C. Waldauf, C.J. Brabec, Appl. Phys. Lett. 81 (2002) 3885.
36. W. Geens, T. Aernouts, J. Poortmans, G. Hadziioannou, Thin Solid Films 403 (2002) 438.

37. G. Yu, A.J. Heeger, J. Appl. Phys. 78 (1995) 4510.
38. J.J.M. Halls, C.A. Walsh, N.C. Greenham, E.A. Marseglia, R.H. Friend, S.C. Moratti, A.B. Holmes, Nature 376 (1995) 498.
39.
40. K.W. Allen, Theories of Diffusion in Handbook of Adhesion by D.E. Packham, John Wiley and Sons, Inc. Hoboken, 2005.
41. R. W. Carpwick, D. F. Ogletree,J. Colloid interface sci.211, 395(1999)
42. O. Pietrement & M. Troyon, J. Colloid Interface Science. 226, 166(2000)
43. Yanfei Ding, Ping Lu, and Qiying Chen*. “Optimizing material properties of bulk-heterojunction polymer filmsfor photovoltaic applications”
44. Mikkel JørgensenÃ, Kion Norrman, Frederik C. Krebs “Stability/degradation of polymer solar cells”Solar Energy Materials & Solar Cells 92 (2008) 686–714
45. E. Klimov, W. Li, X. Yang, G.G. Hoffmann, J. Loos, Macro-molecules 39 (2006) 4493.
46. X. Yang, J. Loos, S.C. Veenstra, W.J.H. Verhees, M.M. Wienk, J.M. Kroon, M.A.J. Michels, R.A.J. Janssen, Nano Letters 5 (2005) 579.
47. K. Sivula, C.K. Luscombe, B.C. Thompson, J.M.J. Frechet, J. Am. Chem. Soc. 128 (2006) 13988.